SKB

TECHNICAL REPORT 97-32

Cement / bentonite interaction

Results from 16 month laboratory tests

Ola Karnland

Clay Technology AB, Lund, Sweden

December 1997

SVENSK KÄRNBRÄNSLEHANTERING AB
SWEDISH NUCLEAR FUEL AND WASTE MANAGEMENT CO

P.O.BOX 5864 S-102 40 STOCKHOLM SWEDEN
PHONE +46 8 459 84 00
FAX +46 8 661 57 19

CEMENT / BENTONITE INTERACTION

RESULTS FROM 16 MONTH LABORATORY TESTS

Ola Karnland

Clay Technology AB, Lund, Sweden

December 1997

Information on SKB technical reports from1977-1978 (TR 121), 1979 (TR 79-28), 1980 (TR 80-26), 1981 (TR 81-17), 1982 (TR 82-28), 1983 (TR 83-77), 1984 (TR 85-01), 1985 (TR 85-20), 1986 (TR 86-31), 1987 (TR 87-33), 1988 (TR 88-32), 1989 (TR 89-40), 1990 (TR 90-46), 1991 (TR 91-64), 1992 (TR 92-46), 1993 (TR 93-34), 1994 (TR 94-33), 1995 (TR 95-37) and 1996 (TR 96-25) is available through SKB.

CEMENT / BENTONITE INTERACTION

-

Results from 16 month laboratory tests

Ola Karnland

Clay Technology AB, Lund, Sweden

December 1997

Keywords: alteration, bentonite, CEC, cement, cristobalite, CSH, dissolution, pH, physical properties, XRD.

ABSTRACT

The work concerns possible bentonite clay mineral alteration in constructions with bentonite in close contact with cement, and the effect of such changes on bentonite buffer properties. The investigation comprises a 16 months laboratory test series with hydrothermal cell tests, percolation tests and diffusion tests. MX-80 Wyoming bentonite was used in all tests. The clay density was 1.8 g/cm^3 after water saturation, and the temperature was held at 40°C in all tests. Two types of artificial cement pore water solutions were used in the percolation and diffusion tests. One simulating pore-water from SULFACEM cement and the other from Aalborg White Portland cement (AWP). The former had a pH of 13.7 mainly due to a high content of potassium hydroxide, and the latter a pH of 12.8. The bentonite was in direct contact to cast AWP cement in the hydrothermal cell tests. The swelling pressure and the hydraulic conductivity were measured continuously in the percolation tests. After termination, the clay was analyzed with respect to changes in element distribution, mineralogy and shear strength. The water solutions were analyzed with respect to pH, cations and major anions. The results concerning chemical and mineralogical changes in the bentonite may be summarized in the following items:

- ion exchange in the montmorillonite until equilibrium with actual cement pore-water ions was reached,
- increase in cation exchange capacity,
- dissolution of original cristobalite,
- increase in quartz content,
- minor increase in illite content,
- minor formation of chlorite,
- formation of CSH(I) (calcium silicate hydrate),
- wash away of CSH-gel into surrounding water.

A large decrease in swelling pressure and a moderate increase in hydraulic conductivity were recorded in the samples percolated by SULFACEM pore-water solution. The mineralogical alterations only concerned a minor part of the total bentonite mass and the changes in physical properties were therefore most likely due to the replacement of the original charge balancing cation by cement pore-water cations. Made comparisons between the current test results and results from 4 month tests indicate that the rates of illite and chlorite formation were reduced during the tests. The presence of zeolites in the clay could not be ensured. However, the finding of CSH material is important since CSH is expected to precede the formation of zeolites.

SAMMANFATTNING

Rapporten behandlar tänkbara lermineralogiska förändringar i konstruktioner där bentonit står i direkt kontakt med cement, och effekten av sådana förändringar på bentonitens buffertegenskaper. Undersökningen innehåller 16 månaders laboratorieförsök med hydrotermal-, genomströmnings- och diffusionsförsök. MX-80 Wyoming bentonit användes i samtliga försök. Bentonitens densiteten efter vattenmättnad var 1.8 g/cm^3, och temperaturen var 40°C i samtliga försök. Två artificiella cementporvatten användes för genomströmnings- och diffusionsförsöken. Ett simulerade porvatten från SULFACEM cement och hade ett mycket högt pH (13.7), huvudsakligen beroende på hög halt av kaliumhydroxid. Det andra simulerade porvatten från Aalborg White Portland cement (AWP) och hade ett pH på 12.8. I hydrotermalcellförsöken stod bentoniten i direkt kontakt med gjuten AWP-cement. Svälltrycket och den hydrauliska konduktiviteten mättes kontinuerligt i genomströmnings-försöken. Då försöken avslutats undersöktes bentoniten med avseende på fysikaliska, kemiska och mineralogiska förändringar. Vattenlösningarna analyserades med avseende på joninnehåll och pH. Förändringarna i bentoniten kan sammanfattas i följande punkter:

- jonbyte i montmorilloniten till jämvikt med cementporvattnets katjoner,
- ökning av katjonbyteskapaciteten,
- upplösning av ursprunglig kristobalit,
- ökning av kvartsinnehållet,
- liten ökning av illitinnehållet,
- liten nybildning av klorit,
- nybildning av CSH(I) (kalcium-silikat-hydrat(I)),
- bortsköljning av CSH-gel till omgivande vattenlöningar.

En långsam men avsevärd minskning av svälltrycket och en måttlig ökning av den hydrauliska konduktiviteten uppmättes i proven som genomströmmades med SULFACEM-lösning. De mineralogiska förändringarna berörde endast en mindre del av bentonitens massa och ändringarna i de fysikaliska egenskaperna beror därför med stor sannolikhet på jonbytet från ursprungsjoner till cementporvattnets joner. En jämförelse mellan de aktuella resultaten med resultat från 4-månaderstester indikerar att bildnings-hastigheten för illit och klorit avtagit markant under försökets gång. Förekomst av zeoliter kunde inte säkerställas i bentoniten. Upptäckten av CSH material är betydelsefull eftersom CSH förväntas föregå bildningen av zeoliter.

TABLE OF CONTENTS

SUMMARY AND CONCLUSIONS

Three different types of alteration tests have been used in this 16 month test series, i.e. hydrothermal cell tests, percolation tests and diffusion tests. In all tests, MX-80 Wyoming bentonite was used at a density of 1.8 g/cm^3 after water saturation, and the temperature was held at 40°C. In the hydrothermal cell tests, the compacted samples were contacted to cast Portland cement and the system was saturated with an artificial ground water solution (NASK). In the percolation tests, compacted bentonite samples were percolated with two different artificial cement water solutions (AWP, SULFACEM) under a water pressure gradient. In the diffusion tests compacted bentonite samples were contacted to artificial cement pore water solutions at the high concentration side and to artificial ground water at the low concentration side. The hydraulic conductivity and the swelling pressure were measured during the whole test period in the percolation tests. After the 16 month of hydrothermal treatment all three types of samples were analyzed with respect to rheological properties, water ratio, element distribution (EA), cation exchange capacity (CEC), mineralogy (XRD) and microstructure (SEM-EDX) according to Figure 1. The water solutions were analyzed with respect to pH, cation and major anion content.

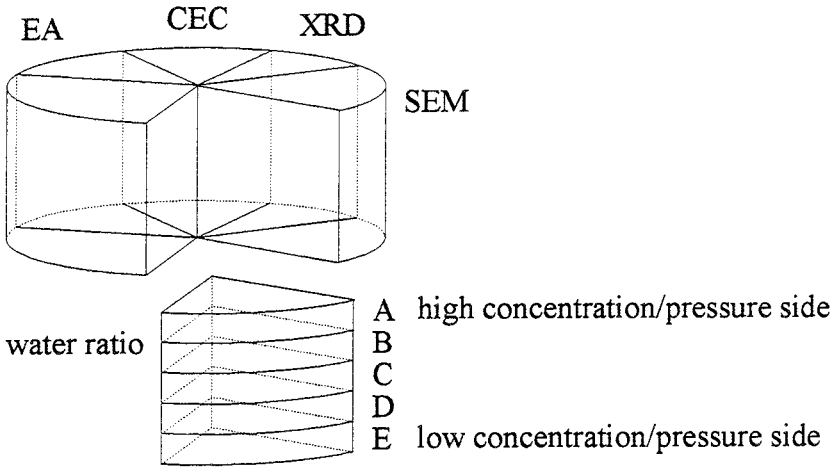

Figure 1. *Schematic drawing of the principle for sampling after test termination. All pieces were divided up into sections from A to E and analyzed by the various techniques.*

The results may be summarized in the following items with respect to chemical and mineralogical changes in the bentonite:

- ion exchange in the montmorillonite with actual cement pore-water ions, likely until equilibrium was reached,
- increase in cation exchange capacity,
- dissolution of original cristobalite,
- increase in quartz content,

- minor increase in illite content,
- minor formation of chlorite,
- formation of CSH(I) (calcium silicate hydrate),
- wash away of CSH-gel into surrounding water.

A large decrease in swelling pressure (Figure 2) and a moderate increase in hydraulic conductivity were recorded in the samples percolated by SULFACEM pore-water solution (sample CB17 and CB27).

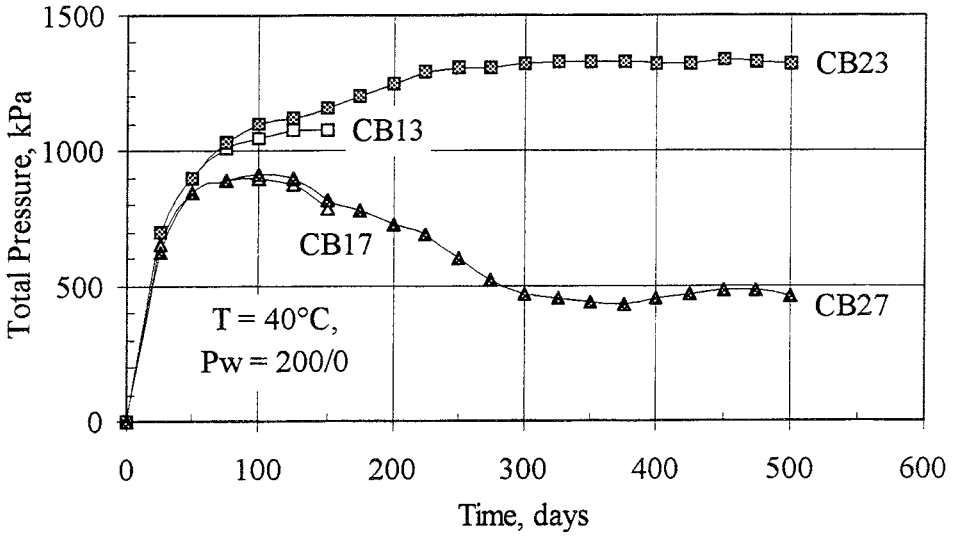

Figure 2. *The total pressure in all percolation samples. The values are reduced and corrected from daily readings.*

The mineralogical alterations only concerned a minor part of the total bentonite mass and the changes in physical properties were likely due to the replacement of original charge balancing cation by cement pore-water cations. Made comparisons between the current test results and results from the 4-month tests indicate that the illite and chlorite formation rates were reduced during the test. Identification of zeolites in the clay could not be ensured. However, the finding of CSH material is important since CSH is expected to precede the formation of zeolites.

1 GENERAL

1.1 BACKGROUND

Bentonite will most probably be used together with concrete for sealing purposes in repositories for spent nuclear waste. The bentonite in close contact with the concrete may be chemically affected in several ways, the most serious alteration being an attack on the montmorillonite clay crystal lattice, while change of the type of adsorbed cations, e.g. from sodium to calcium, is considered as a minor problem in the case of highly compacted bentonite clay. The scope of this study was to identify degrading processes of this kind and to determine what there effects on the physical properties of the bentonite clay may be. The report concerns the results from the 16 month test series of the "Cement-Clay interaction" project, equally financed by NAGRA and SKB.

1.2 TEST LAYOUT

Three different types of hydrothermal tests have been used in this 16 month test series, i.e. hydrothermal cell tests, percolation tests and diffusion tests (table 1-1). In the hydrothermal cell tests, compacted bentonite samples were contacted to cast Portland cement and the system was saturated with artificial ground-water solution (NASK). In the percolation tests compacted bentonite samples were percolated with two different artificial cement water solutions (AWP, SULF) under a water pressure gradient. In the diffusion tests compacted bentonite samples were contacted to artificial cement pore water solutions at the high concentration side and to artificial rock ground water at the low concentration side. The temperature was held at 40°C in all tests. The hydraulic conductivity (hc.) and the swelling pressure (sp.) were measured during the whole test period in the percolation tests. After the 16 month of hydrothermal treatment all three types of samples were analyzed with respect to rheological properties, water ratio (w), element distribution (G2), cation exchange capacity (CEC), mineralogy (XRD) and microstructure (SEM-EDX). The surrounding water solutions were analyzed with respect to ion content (kat., an.) and pH.

Table 1-1. Showing the conducted tests. Figures between [ ] show the number of analyses in each sample. c denotes continuously, m denotes monthly and s denotes sections.

sample	Temp	sol.	Sample	hc	sp	rheo.	w	kat.	an.	pH	G2	CEC	XRD	SEM
21	40°	NASK	hydro.	-	-		[5]	[1]	[1]	[1]	[3]	[3]	[3]	[s]
22	"	"	"	-	-	[3]		[1]	[1]	[1]				
23	"	AWP	perc.	c	c		[5]	[9]	[2]	[m]	[5]	[5]	[5]	[s]
24	"	"	"	c	c	[5]								
25	"	"	diff.	-	-		[5]	[9]	[2]	[m]	[5]	[5]	[5]	[s]
26	"	"	"	-	-	[5]								
27	"	SULF	perc.	c	c		[5]	[9]	[2]	[m]	[5]	[5]	[5]	[s]
28	"	"	"	c	c	[5]								
29	"	"	diff.	-	-		[5]	[9]	[2]	[m]	[5]	[5]	[5]	[s]
30	"	"	"	-	-	[5]								

1.3 MATERIALS

The bentonite used in all tests was MX-80 Volclay from American Colloid Co., Wyoming. The material is dominated by natural sodium montmorillonite clay (~ 75% by weight), which is responsible for the desired physical properties. The rest consists of quartz (~15%), feldspars (~7%), carbonates (~1.4%) sulfides (~0.3%), organic carbon (~0.4%) and around 2% other minerals. Appendix A1 shows XRD-diagram of the bulk material and the chemical composition is given in Table 1-2. Dispersed in distilled water the clay fraction (d < 2 μm), make up around 80%, of which 90-95% are in the minus 0.2 μm fraction after active dispersion. The mean mineralogical composition of the montmorillonite part is given by:

$$(Al_{3.10}\,Fe^{3+}_{0.4}\,Fe^{2+}_{0.02}\,Mg_{0.48})\;(Si_{7.92}\,Al_{0.08})\,O_{20}\,(OH)_4\;\;Na_{0.48}\,Ca_{0.04}\,Mg_{0.02}$$

octahedral cations | tetrahedral cations | structural O and OH | exchangeable cations

The cation exchange capacity is around 80 meq/100 g material in the bulk material and around 110 meq/100 g clay in the minus 2μm fraction. The natural exchangeable cations are sodium (~85%), calcium (~10%), magnesium (~4%) and small amounts of potassium (~0.3%). The specific surface area is around 550 m^2/gram material and the grain density is around 2.75 g/cm^3 (Müller-Vonmoos, 1983).

In order to get a more defined material, suited especially for the diffusion experiments, the bulk material was converted to a maximum sodium state by use of NaCl. Approximately 50 g clay was dispersed in 1 L 1M NaCl solution and left overnight. The supernatant was removed and replaced by 0.1 M NaCl solution and the suspension was centrifuged in order to give a fixed clay cake in the centrifuge bottle and the supernatant was removed.

The dispersion/centrifugation in 0.1 M NaCl solution was repeated further 2 times (3 times in total). The bentonite was finally dried at 60°C and gently ground to a grain size which was similar to the original MX-80 material.

Table 1-2. Results from ICP-AES element analyses of standard MX-80 material expressed as oxides. MX-80 c denotes results from the minus 2 μm fraction. LOI denotes the loss of ignition (at 1050°C). All figures indicate percent by weight (Karnland 1995).

material	SiO_2	Al_2O_3	Fe_2O_3	TiO_2	MgO	CaO	K_2O	Na_2O	LOI
MX-80	63.4	20.0	4.4	0.2	2.64	1.42	0.48	2.53	6.1
MX-80 c	62.3	20.8	3.7	0.17	3.04	1.01	0.31	2.09	5.6

The cement used for the hydrothermal cell tests was an iron- and aluminum-poor version from Aalborg, Denmark, labeled Aalborg White Portland (AWP) Table 1-3. An elemental analysis[1] gave the Bogue composition: C_3S (61%w), C_2S (24%w), C_3A (4.4%w), C_4AF (1.0%w), $CaSO_4$ (3.2%w) and free CaO (3.5%w) (Hjorth 1988). Results from ICP-AES element analyses of AWP cement and Na converted MX-80 material are shown in Table 1-3. The water solution used in the hydrothermal tests was an artificial sodium-dominated groundwater, here called NASK water (Table 1-4). This solution was also used in the percolation and diffusion tests at the "low pressure/concentration side". At the opposite side, solutions representing pore water from the two cement types AWP and SULFACEM were used. The main difference between the two cement types, is the high content of Na^+ and K^+ in the pore water of the latter, giving the pore water solution a very high pH (~13.7). The compositions of the solutions are given in Table 1-5 and 1-6.

Table 1-3. Results from ICP-AES element analyses of AWP cement and Na converted MX-80 material used in this study expressed as oxides. LOI denotes the loss of ignition (at 1050°C). All figures indicate percent by weight.

material	SiO_2	Al_2O_3	Fe_2O_3	TiO_2	MgO	CaO	K_2O	Na_2O	LOI
AWP	24.4	1.91	0.15	0.01	0.61	59.1	0.05	0.07	1.6
MX-80 Na	61.3	19.0	4.05	0.18	2.42	0.78	0.51	4.01	6.4

[1] Cement nomenclature: C = CaO, S = SiO_2, A = Al_2O_3, F = Fe_2O_3, H = H_2O, S = S_3

Table 1-4. The composition of the NASK test solution.

Ion	charge	mole w. g	conc. mg/l	conc. mmol/l	El. bal. meq
Na^+	1	23	3220	140	140
K^+	1	39.1	78	2	2
Ca^{2+}	2	40.1	802	20	40
Mg^{2+}	2	24.3	97	4	8
Sum			4197	166	190
Cl^-	-1	35.5	6390	180	-180
HCO_3^-	-1	61	122	2	-2
SO_4^{2-}	-2	96	384	4	-8
OH^-	-1	17		0	0
Sum			6896	186	-190
Total			11093	352	0

Table 1-5. Composition of the AWP water solution used in the percolation and diffusion experiments. "s" denotes saturated with respect to $Ca(OH)_2$.

Ion	charge	mole w. g	conc. mg/l	conc. mmol/l	El. bal. meq
Na^+	1	23	4163	181	181
K^+	1	39.1	78	2	2
Ca^{2+}	2	40.1	s	s	s
Mg^{2+}	2	24.3	0	0	0
Sum			4241	183	183
Cl^-	-1	35.5	5041	142	-142
HCO_3^-	-1	61	0	0	0
SO_4^{2-}	-2	96	384	4	-8
OH^-	-1	17	561	33	-33
Sum			5986	179	-183
Total			10227	362	0

Table 1-6. Composition of the SULFACEM water solution used in the percolation and diffusion experiments. "s" denotes saturated with respect to $Ca(OH)_2$.

Ion	charge	mole w. g	conc. mg/l	conc. mmol/l	El. bal. meq
Na^+	1	23	4761	207	207
K^+	1	39.1	17321	443	443
Ca^{2+}	2	40.1	s	s	s
Mg^{2+}	2	24.3	0	0	0
Sum			22082	650	650
Cl^-	-1	35.5	5041	142	-142
HCO_3^-	-1	61	0	0	0
SO_4^{2-}	-2	96	384	4	-8
OH^-	-1	17	8500	500	-500
Sum			13925	646	-650
Total			36007	1296	0

1.4 HYDROTHERMAL CELL TESTS

In the hydrothermal cell tests, cement/bentonite samples were confined in cylindrical sample holders made of Teflon and allowed to interact with surrounding NASK water solution through Teflon filters at both ends (Figure 1-1), The AWP Portland cement had a water/cement ratio of 0.8 and was cast in the Teflon cell and allowed to harden in NASK water solution for 1 month before the bentonite was placed. The cement occupied half of the cell and bentonite was compacted to fill the remaining space with a density corresponding to 1.8 g/cm^3 after water saturation.

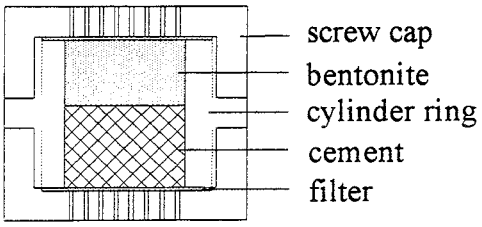

Figure 1-1. *Teflon sample holder used in the hydrothermal cell tests.*

Two samples were prepared and placed in hydrothermal cells, which consisted of cylindrical stainless steel tubes lined with Teflon and filled with 500 cm^3 NASK water solution (Figure 1-2). The reaction space was pressurized by an external water pressure, transmitted by a Teflon piston. The samples were allowed to hydrate for 2 weeks in the cells and then placed in ovens, which were slowly heated to 40°C. In order to create similar

conditions as in earlier test series, the water pressure was held at 2 MPa during the whole test period.

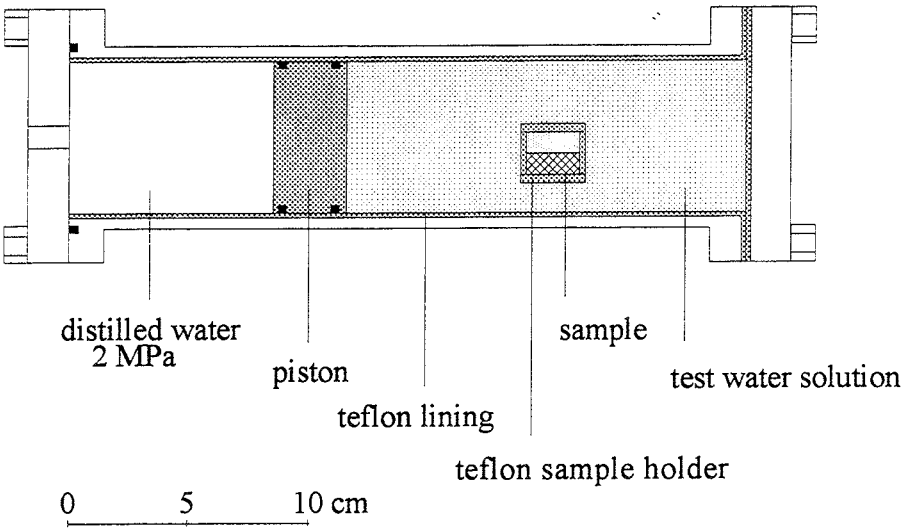

Figure 1-2. *The hydrothermal cell made of acid proof stainless steel and lined with Teflon in order to make the system chemically inert .*

After hydrothermal treatment for 16 months, the temperature was lowered and the water pressure slowly reduced to 100 kPa. The test solutions as well as the samples were only exposed to air for a few minutes during the opening, and thereafter kept in airtight boxes until they were analyzed.

1.5 PERCOLATION TESTS

Air-dry bentonite was compacted to a density corresponding to 1.8 g/cm^3 after water saturation. The samples were placed in 4 cylindrical sample holders of stainless steel with a diameter of 50 mm and a height of 20 mm (Figure 1-3). The bentonite was confined at both ends by stainless steel filters, which were supported by a steel plate at one end and by a piston at the other. Both filters were connected to water by an inlet and an outlet tube in order to circulate the different solutions through the filters, and thereby keeping the solution concentrations constant. The pistons were connected to force transducers, by which the total pressure from the samples could be recorded.

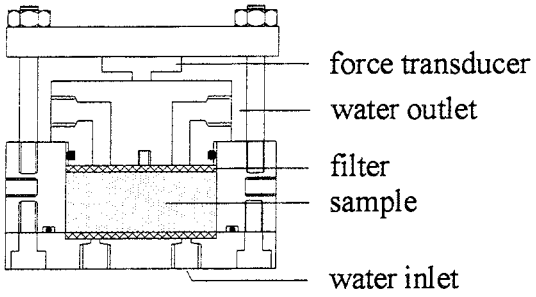

Figure 1-3. *Cell for percolation and diffusion tests.*

The samples were saturated with NASK water solution under a water pressure of 100 kPa at both sides (Figure 1-4). After approximately 1 week, the total pressures, measured by the pressure transducers, were constant and the water pressure was then increased to 200 kPa at the inlet side. After 50 days the temperature was increased to 40°C and the samples were contacted to the cement test solutions. Recordings of water flow and pressure were made daily during the 16 months test period. Circulation of the test solutions through the filters was made weekly and the test solutions were changed 4 times during the test period in order to maintain the intended concentrations in the filters. Element analyses, including pH check, of the solutions were made at each change.

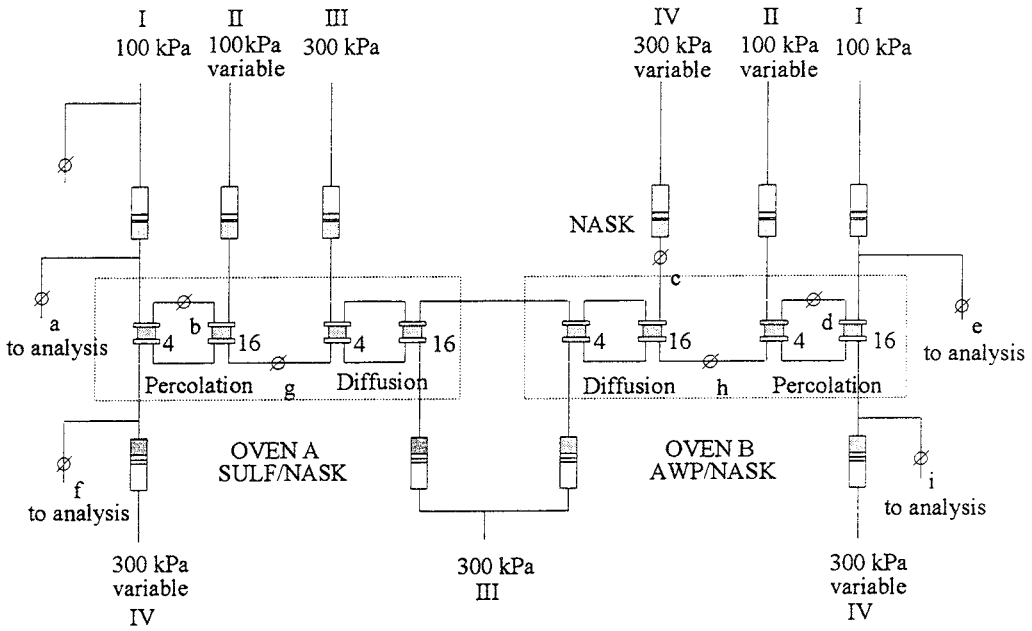

Figure 1-4. *The percolation and diffusion test set up. The left side of the scheme was contacted to the SULFACEM cement solution and the right side to the AWP cement solution. The pressurizing system was used in a "cross-connected" fashion, in order to maintain equal gradients over the percolation samples and no gradient over the diffusion test samples.*

1.6 DIFFUSION TEST

The preparation of the diffusion test samples was identical to the preparation of the percolation tests samples, except that the clay was saturated with distilled water before it was contacted to the test solutions. The element transport into the samples hence took place solely by diffusion. The test equipment was also identical except that no pressure transducers were used in the diffusion experiments. A moderate water pressure (300 kPa) was applied on both sides in order to keep the system well hydrated and to minimize air leakage into the system. The artificial cement pore-water solutions were percolated through the filters weekly, and changed 4 times during the test period in order to maintain the intended concentrations in the filters. Element analyses, including pH check, of the solutions were made at each change.

2 TESTS AND ANALYSES

2.1 PHYSICAL PROPERTY TESTS

2.1.1 Hydraulic conductivity

The water flow through the samples in the percolation tests was recorded in two separate ways. At the low pressure side, the samples were connected through tubes to approximately 0.5 liter NASK solutions placed in the cylindrical Plexiglas vessels. The solutions were pressurized by Plexiglas pistons which in turn was pressurized by distilled water. Compressed air was used to pressurize the distilled water in tubes, which made it possible to read the meniscus positions and thereby to calculate the hydraulic conductivities in the samples. At the high pressure side, the water pressure was achieved by a pressure/volume control system (GDS) with a resolution of 1 mm^3 and 1 kPa. The water volume change, at the intended constant water pressure, was recorded by a computer, which made it possible to calculate the hydraulic conductivities. The former technique overestimates the conductivity if there is some leakage in the system, and the latter underestimates it. However, both systems are sensitive to room temperature changes because of the large water volumes involved. The hydraulic conductivities (k, m/s) were calculated according to Darcy's law:

$$k = \frac{V \cdot l}{A \cdot h \cdot t},$$

where V is the percolated water volume (m^3), l is the sample length (m), A is the sample area (m^2), h is the hydraulic pressure (meter water column) and t is time (s).

2.1.2 Swelling pressure

Force transducers were placed between the piston and the base plate of the percolation tests cells in order to measure the total axial force from the samples (Figure 1-3). The total pressure (P_{tot}) was calculated according to:

$$P_{tot} = \frac{F}{A},$$

where F (N) is the recorded force and A (m^2) is the piston/bentonite contact area. Approximate swelling pressure may be calculated by subtracting the applied mean water pressure from the recorded total pressure according to previous laboratory tests. Computer recordings were made parallel to the water volume recordings, i.e. every half hour during the water saturation period and thereafter twice a day.

2.1.3 Water ratio

After test termination approximately 1/6 of each sample was cut out for determining the water ratio (w) in accordance with Figure 2-1. The samples were split in 5 sections along the axial direction, which represented the concentration or pressure gradient direction. Around 1 gram of material from each slice was dried in an oven at 105°C for 24 hours and the water ratio was calculated from:

$$w = \frac{m_w}{m_s},$$

where m_w is the water loss and m_s is the remaining solid. The initial clay density of 1.8 g/cm^3 corresponds to water ratio of 43% after complete saturation with distilled water.

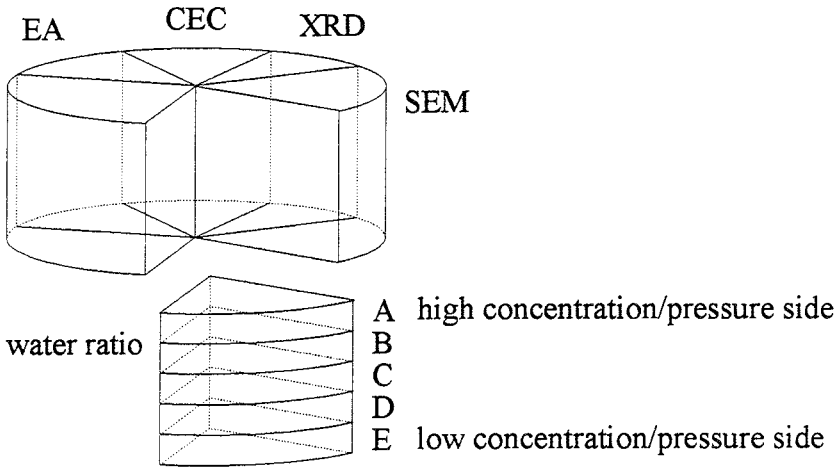

Figure 2-1. *Schematic drawing of the principle for sampling after test termination of the percolation and diffusion tests.*

2.1.4 Rheology

In order to determine the shear strength and also to identify possible cementations a Bohlin rheometer was used (Figure 2-2). The test samples were placed in a sample holder, and a laboratory vane bore mounted on a torsion element was pressed into the samples. The sample holder was then slowly rotated by an electrical motor and the torque was recorded every second by a computer. Three sections were tested along the axial direction in the samples from hydrothermal cell tests and five in all other samples. After the first level had been sheared the level was removed and the next level was tested.

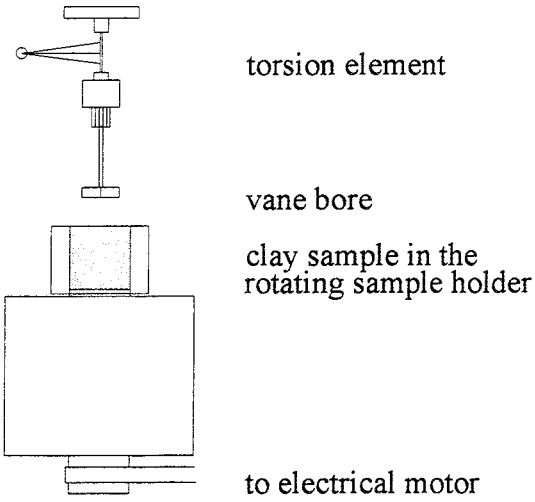

Figure 2-2. *Schematic drawing of the central part of the rheometer.*

2.2 WATER ANALYSES

2.2.1 pH of test water solutions

All measurements were made by use of a standard Metrohm 632 pH-meter equipped with a glass electrode. The solutions from the hydrothermal tests were transferred from the test cells to airtight bottles at test termination and pH was determined as soon as the solutions had cooled down to 25°C. The test solutions in the percolation and diffusion tests were checked with respect to pH approximately every second month, mainly in order to ensure that no major air leakage (CO_2) had taken place. pH was further measured in conjunction with the chemical analyses of the test solutions.

2.2.2 Elements analyses of test water solutions

The NASK solutions and the two artificial cement solutions in the percolation and diffusion experiments were replaced 4 times during the test period. Some of the replaced and all final solutions were analyses by use of ICP-AES technique in order to quantify the main element and by titration in order to quantify the main anions (Cl^-, SO_4^{2-}, and HCO_3^-).

2.3 MINERALOGICAL ANALYSES

2.3.1 Elements

Five specimens from each test sample, extracted as for the water ratio determination (Figure 2-1), were used for the chemical analyses of the solid phase of the samples. The sampling was made immediately after tests termination in order to avoid pore water redistribution. The specimens were melted in a mixture of lithium carbonate and dibortrioxide, and then dissolved in nitric acid before the analyses, which were made by use of ICP-

AES technique. The loss of ignition (LOI) values show the relative amount of volatile components at heating to 1050°C. The content of elements are given in the form of oxides, and in order to make direct comparison between the samples possible, the main element values have been corrected with respect to the LOI. Two determinations, including new melting and dissolution, were made on a few specimens.

2.3.2 Cation Exchange Capacity (CEC)

Formation of zeolites and illite are expected to be favored by high pH conditions. The CEC is expected to increase if zeolites are formed or if the lattice charge of the smectite components is increased. On the other hand, a decrease is expected if the montmorillonite component is transformed into illite, either by direct transformation through fixation of potassium, or by dissolution and neoformation.

After test termination approximately 1/6 of each sample was cut out for the CEC analyzes in accordance with Figure 2-1. The analyses were made on the clay fraction in order to enhance the precision, which means that conceivable large neoformed grains may be overlooked. The analysis method involves ion exchange from the original cations to NH_4^+ by repeated washings with ammonium acetate at pH 7. The supernatants from the washings were analyzed with respect to the concentration of the extracted cations, which may originate from exchange positions and also from other possibly dissolved substances. The results are presented as individual cations and as the sum of extracted cations (SEC). The samples were then washed 3 times with 2-Propanol and finally, the NH_4^+ was replaced by a strong NaCl-solution (10% by weight). The supernatants from the NaCl-solutions were analyzed with respect to NH_4^+ -concentration and the results were used for calculation of the CEC-values. Reference tests showed that the resolution of the CEC analyses was better than 5 meq/100 g clay and that $Ca(OH)_2$ or $CaCO_3$ precipitation did not disturb the analyses significantly.

2.3.3 X-ray diffraction (XRD)

After test termination approximately 1/6 of each sample was cut out for the XRD analyzes in accordance with Figure 2-1. Material from each sample section was analyzed without any separation since the aim was to detect possible mineralogical changes which may take place in any size fraction of the original bentonite material. The specimens were crushed in an agate mortar and gently packed into the specimen holder in order to avoid orientation of the mineral grains. The thereby random orientation suppresses the strong basal reflections from the montmorillonite in the bentonite, and increases the probability of complete "fingerprints" from all involved minerals. The analyses were made by use of a Siemens D 500 machine equipped with a copper anode (Cu, Kα radiation). The scanning interval was 3 to 65° (2Θ) and the scanning frequency was 100 intensity measurements

per 1° (2Θ). In the presented diffractograms (Appendix A) the curves have been smoothed by showing each point as a mean value of ± 2 point values.

2.3.4 Scanning electron microscopy (SEM-EDX)

Analyses made by use of SEM-EDX of natural bentonite are very precise and may detect non-representative structures and minerals, since a large number of minerals are present in the original MX-80 material. In order to claim that a certain mineral has been neoformed a large number of findings has consequently to be made. On the other hand, neoformed structures may elude detection since the analyses always concern a very small volume of a studied specimen. In order to get the analyses as representative as possible the specimens were surveyed by use of backscatter technique and EDX mapping at low magnification. Interesting parts were studied in detail by use of EDX spot analyses at high magnification (up to 5 000 times), and characteristic morphological structures were documents by b/w photos.

The preparation of the SEM specimens were made in the following way:

- Specimens were cut from undisturbed samples at test termination,
- rapidly frozen in liquid nitrogen (N_{liq}),
- freeze dried for 24 h at -20°C and 1 Pa,
- broken, in order to expose fresh surfaces,
- sputter coated with gold to a thickness of 20 nm,
- fixed to an aluminum stub by use of carbon glue.

The microstructure study was made by use of a Phillips 515 SEM microscope and the micro element analyze by use of a LINK 2000. The energy dispersive X-ray (EDX) detector was equipped with a beryllium window which limits the analyses to elements with $Z > 11$ (Na).

3 RESULTS

3.1 PHYSICAL PROPERTIES

3.1.1 Swelling pressure and hydraulic conductivity

MX-80 bentonite, with a density of 1.8 g/cm³ after water saturation, normally has a swelling pressure around 800 kPa, and a hydraulic conductivity around $1*10^{-12}$ m/s (Figure 3-1 and 3-2).

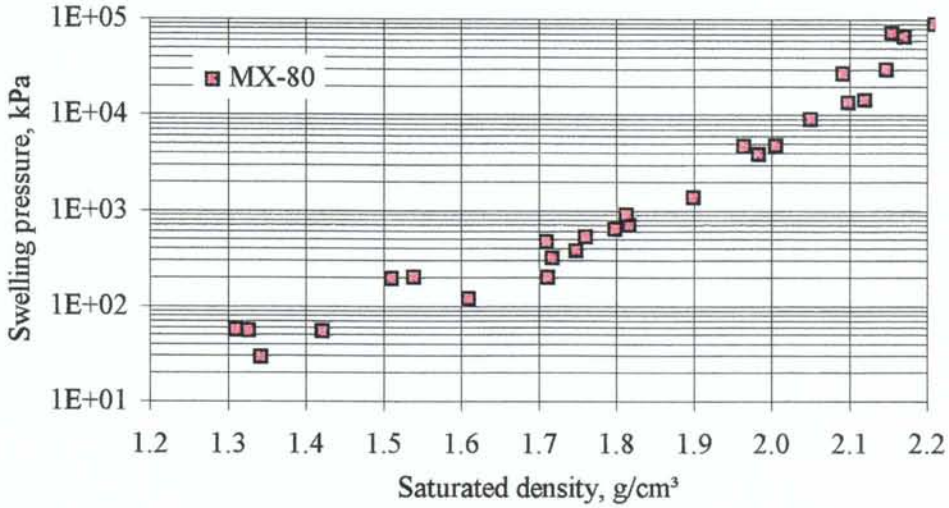

Figure 3-1. *Results from oedometer tests showing swelling pressure as a function of sample density for MX-80 bentonite saturated with distilled water. Compilation of CT oedometer test results from 1989 to 1993 according to test technique described in Karnland 1994.*

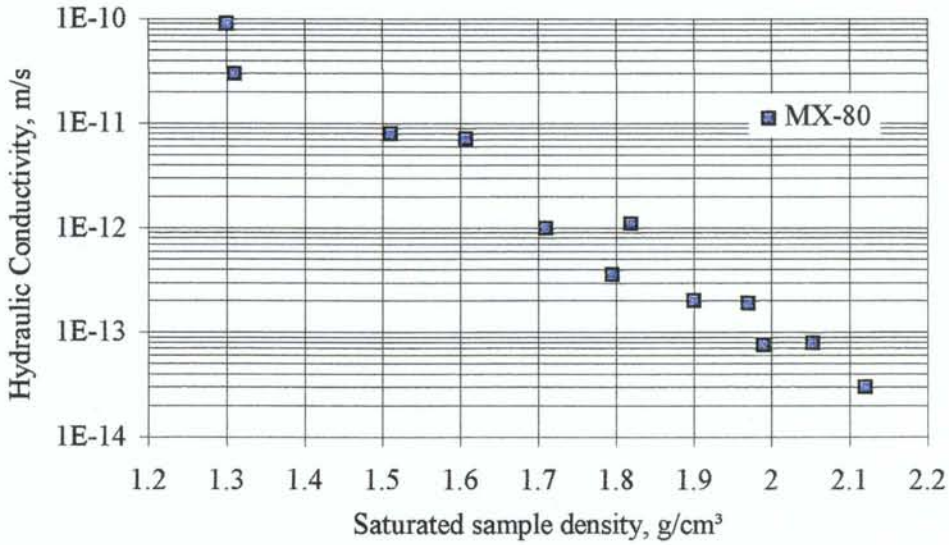

Figure 3-2. *Results from oedometer tests showing hydraulic conductivity as a function of sample density for MX-80 bentonite saturated with distilled water. Compilation of CT oedometer test results from 1989 to 1993 according to test technique described in Karnland 1994.*

In this study, the samples had a measured stable swelling pressure of around 350 kPa one week after they were contacted with NASK water solution without backpressure (Figure 3-3). The water pressure was then increased to 200 kPa at the high pressure side and the percolating solution volume was measured in order to determine the hydraulic conductivity. As a consequence, the swelling pressure in all samples started to slowly increase and the hydraulic conductivity decreased in a corresponding way. After 40 days from saturation start the total pressure in all samples had increased to around 800 kPa and the hydraulic conductivities had decreased to around $1*10^{-12}$ m/s, which may be seen as typical values for the ambient test conditions. The water pressure was therefore reduced to zero and stable swelling pressures around 700 kPa were recorded. The samples were then contacted with the cement solutions on one side according to Figure 1-4, and the temperature was increased to 40°C. A water pressure of 300 kPa was applied at the cement solution side and of 100 kPa at the NASK solution side. An additional slow increase in swelling pressure was noticed in all samples parallel to an additional reduction in hydraulic conductivity.

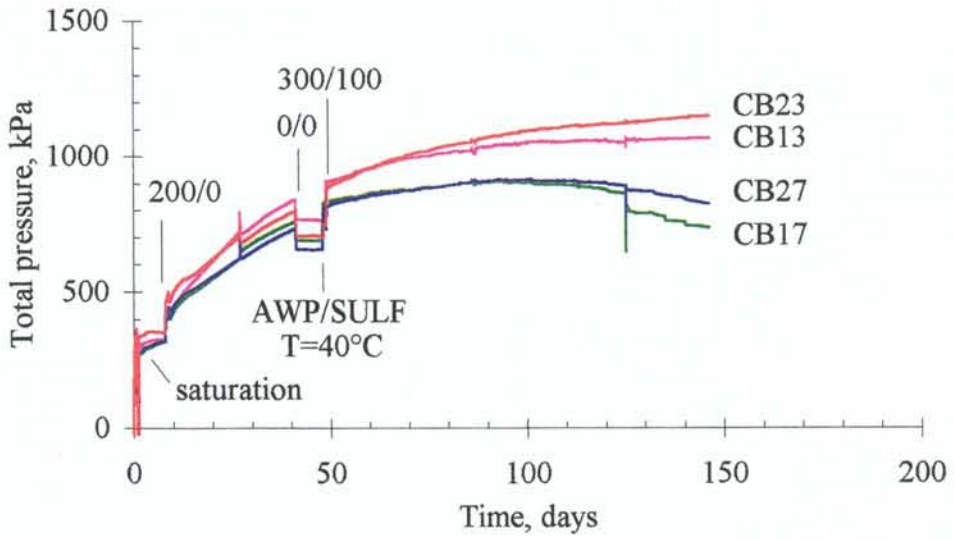

Figure 3-3. *Total pressure in all percolation samples during the saturation and test start period. The figures above the curves denote the applied water solution pressure.*

The required time to reach the swelling pressure peak values in all samples, and the obvious change in swelling pressure, especially in the "AWP samples", indicate that the pressure increase was not only an effect of the applied water pressure but to a larger extent an effect of equilibration with the surrounding solutions (Figure 3-4). After approximately 100 days from test start the total pressure in the sample percolated with SULF cement pore water began to decrease. An equilibrium was reached at around 450 kPa after approximately 300 days from test start. The swelling pressure, calculated by subtracting the mean pore water pressure from total pressure, was accordingly as low as around 250 kPa. The decrease is likely to be attributed ion exchange in the montmorillonite from sodium to potassium and the high ion strength in the SULF solution (Karnland, 1994). Consequently,

the swelling pressure reduction is likely not related to mineralogical changes in the montmorillonite lattice.

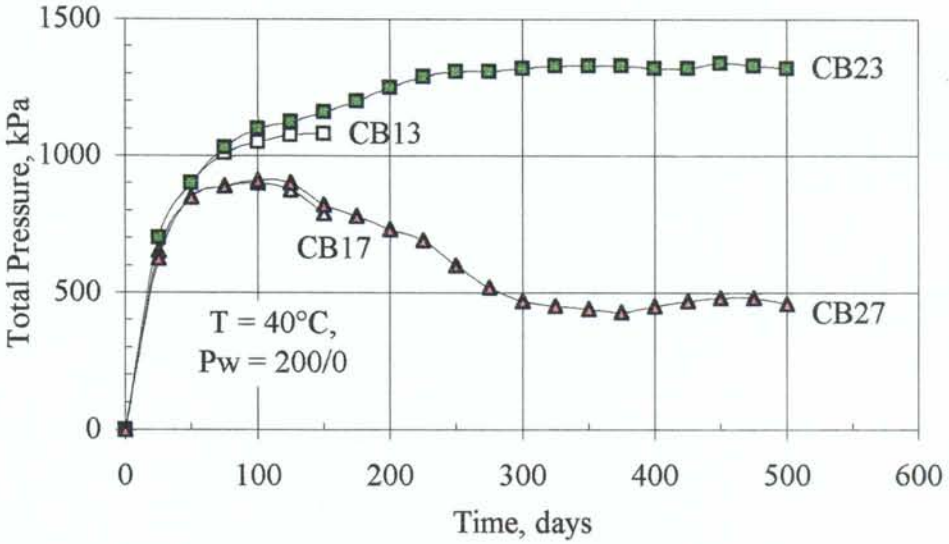

Figure 3-4. *The total pressure in all percolation samples. The values are reduced and corrected from daily readings.*

The measured final hydraulic conductivities were in general typical for bentonite with the actual clay density (Figure 3-2). However, the individual changes with time are significant. The decrease during the first test period may be explained by a homogenization of the clay, which in turn may be due to both equilibration with the surrounding solutions and to the temperature increase (Figure 3-5). The hydraulic conductivity in sample CB27 started to slowly increase after approximately 120 days while it was constantly low in sample CB23. The difference is likely an effect of a successive cation exchange from sodium to potassium in the latter samples.

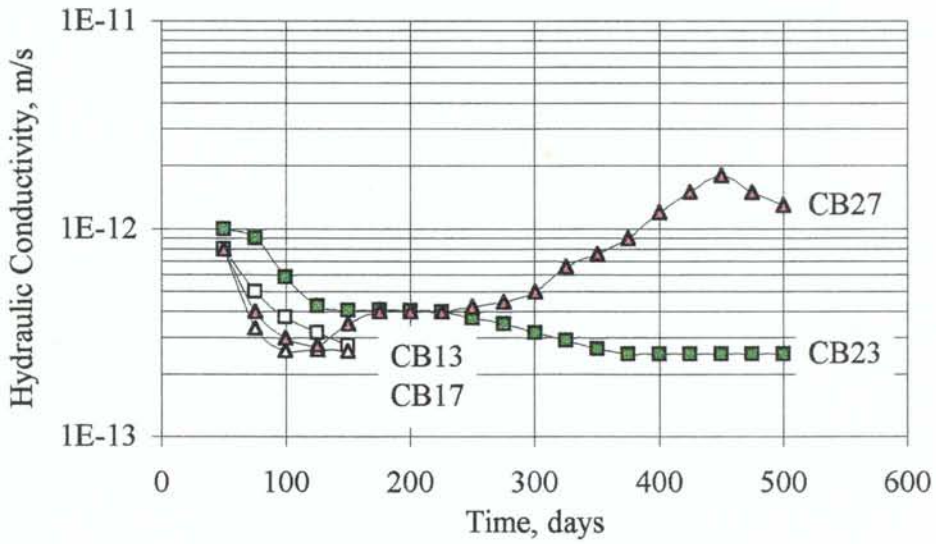

Figure 3-5. *The hydraulic conductivity evolution after percolation start with the cement pore water solutions. The data are corrected and reduced from daily readings.*

The total amount of percolated water was 0.108 liter in sample CB23 and 0.232 liter in sample CB27 corresponding to a total mass of dissolved ions of 1.27 g and 8.40 g respectively. The much higher value in CB27 is due to the higher ion strength in the SULF solution (Figure 3-6).

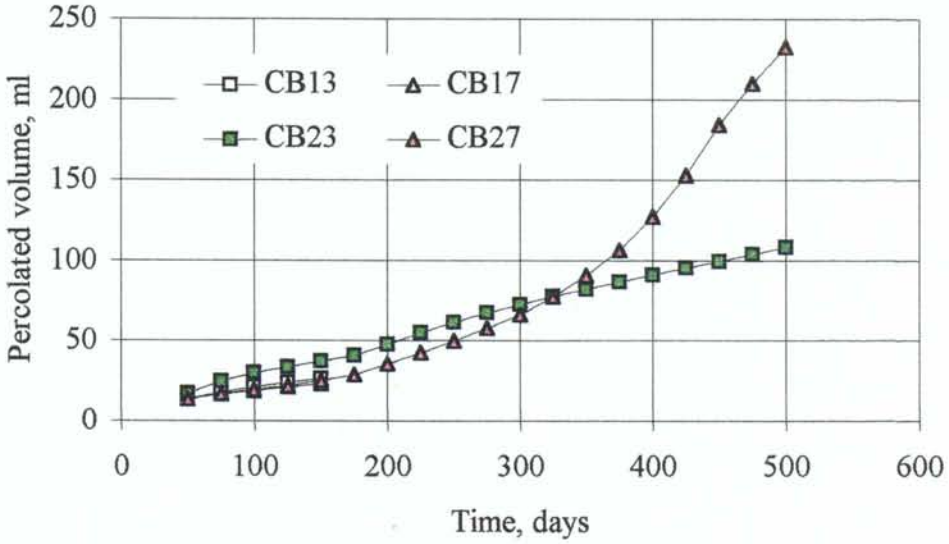

Figure 3-6. *Total percolated solution volume in the four percolation tests.*

3.1.2 Water ratio

The initial clay density corresponds to a theoretical water ratio of 43.2%. The measured values in sample CB21 were generally significantly higher, likely due to long term deformation of the Teflon sample holder. The four other samples, which were confined in steel sample holders, showed a general trend towards higher water ratios at both ends and with somewhat higher mean values than the theoretical value (Figure 3-7).

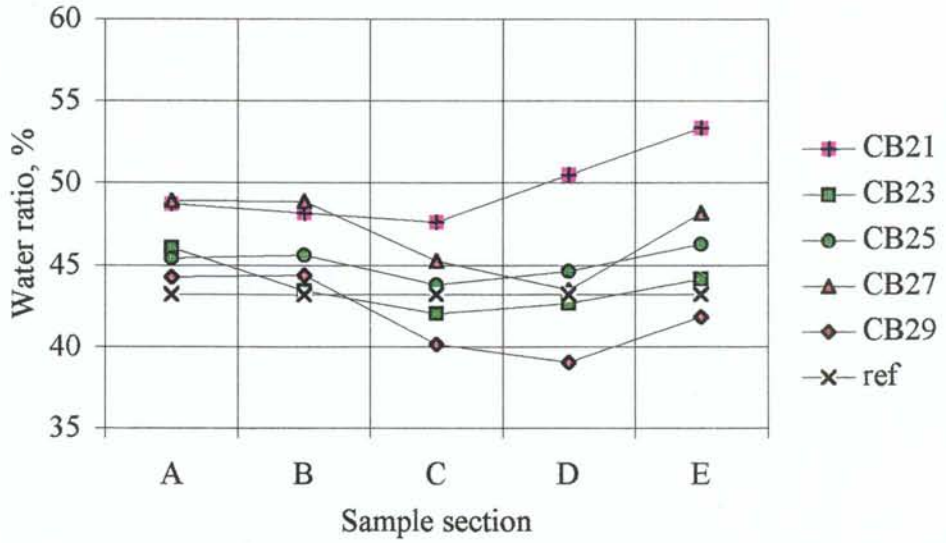

Figure 3-7. *Water ratio for all samples in the 16 month test series. Section A represents the "cement" side of the samples.*

Both conditions were especially pronounced in sample CB27 in which the mean water ratio was 46.9%. The displacement of the piston, due to the deformation of the force transducers, was less than 50 μm and this would give a change in water ratio by less than 0.5%. The major cause of the measured increase in water ratio is consequently a reduction of the solid phase. The change in sample CB27 corresponds to a theoretical loss of 2.2 grams, which in turn corresponds to 4.5% of the original solid mass.

3.1.3 Rheology

Figure 3-8 shows the shear stress progress in sample CB29 during the shearings. All section in this sample have a shear strength (maximum shear stress) in the range of 140 and 180 kPa and the peak value at an angle of around 5°. Figure 3-9 shows the shear strength for all samples in the test series. The recorded differences both between and within the various samples are rather small and probably more related to minor density variations than to true rheological changes induced by the cement solutions.

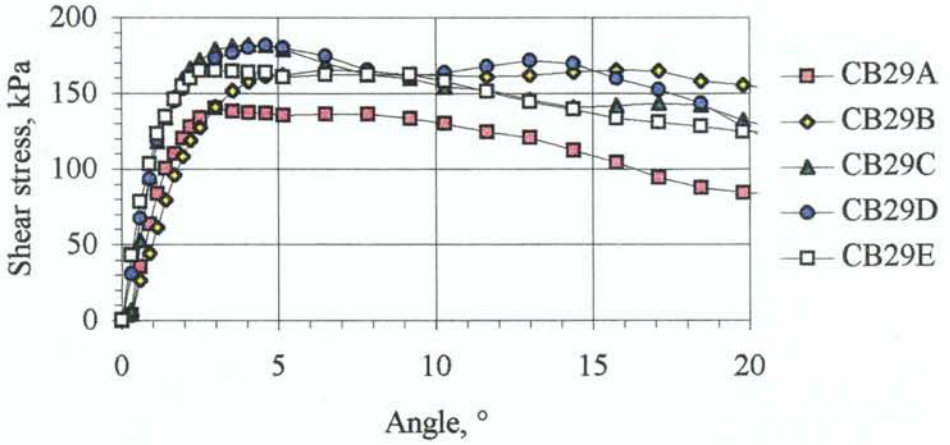

Figure 3-8. *Shear stress progress during shearing in sample CB29.*

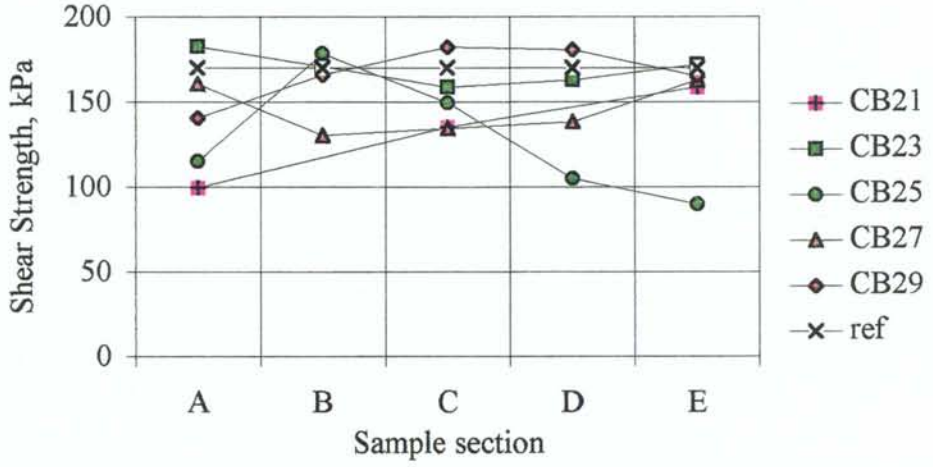

Figure 3-9. *Shear strength of all samples in the 16 month test series. Section A represents the "cement" side of the samples.*

3.2 WATER ELEMENT ANALYSES

3.2.1 Hydrothermal cell test

The analyses of the NASK water solution from the hydrothermal tests showed only minor anion concentration changes (Table 3-1 and Appendix B). The increase in Na^+ concentration and the decrease of other cations, especially the divalent calcium and magnesium, are likely due to ion exchange in the clay. The differences between the two test solutions are reasonably small. The pH discrepancy is however noteworthy.

Table 3-1. Original NASK solution content and analyzed ion content changes in test solutions at termination of the hydrothermal cell tests .

sample	pH	alk	OH^-	Cl^-	SO_4^{2-}	HCO_3^-	Ca^{2+}	Fe^{3+}	K^+	Mg^{2+}	Na^+	Si	total
		mg	mg	mg	mg	mg	mg	mg	mg	mg	mg	mg	mg
NASK	7.7		0	3195	192	60	400	0	39	49	1610	0	
CB21	7.6	25	0	55	3	-36	-140	0	-4	-19	165	2	27
CB22	10.3	17	2	-95	-17	-49	-126	0	-4	-32	140	0	-181

sample	pH	alk	OH^-	Cl^-	SO_4^{2-}	HCO_3^-	Ca^{2+}	Fe^{3+}	K^+	Mg^{2+}	Na^+	charge
		mmole	mmole	mmole	mmole	mmole	mmole	mmole	mmole	mmole	mmole	meq
NASK	7.7	1.00	0.00	90.00	2.00	1.00	10.00	0.00	1.00	2.00	70.00	0.00
CB21	7.6	-0.59	0.00	1.55	0.03	-0.59	-3.50	0.00	-0.10	-0.79	7.17	-2.52
CB22	10.3	-0.73	0.10	-2.68	-0.18	-0.82	-3.15	0.00	-0.10	-1.30	6.09	0.84

3.2.2 Percolation and diffusion tests

The pH in the artificial cement solutions was only slightly reduced during the test period which is of vital importance for the test result (Appendix D). The lowest pH value in the AWP solutions was 12.6 and in the SULF solutions 13.1 (Appendix B). Substantial uptake of carbon dioxide was apparent especially in the SULF solutions. However, the difference between various analyses indicate that the uptake may have taken place after the solutions were removed from the test equipment. The low content of silica, despite conflicting results from supporting analyses, may be due to precipitation of e.g. calcium silicates which probably were overlooked by the present water analyses.

Most changes were logically larger in the solutions contacted to the percolated samples (CB23 and CB27) compared to the changes in the solutions contacted to samples where only diffusion took place (CB25 and CB29) (Figure 3-10 and 3-11). The most significant changes seems to be a transport of potassium from the SULF solution into the clay samples and a sodium transport into the NASK solution. A more general ion exchange seems to have taken place in the clay leading to sodium increase and to decrease of especially divalent ions in all solutions.

Table 3-2. Approximate cumulative changes of total ion content in solutions surrounding sample CB23. Calculated from the five successive water analyses.

CB23	alk.	OH^-	Cl^-	SO_4^{2-}	HCO_3^-	Ca^{2+}	Fe^{3+}	K^+	Mg^{2+}	Na^+	Si	mg
days	mg	mg	mg	mg	mg	mg	mg	mg	mg	mg	mg	total
0	-1	0	0	0.0	0	0	0.0	0	0.0	0	0.0	0
95	500	-17	447	-1.8	34	0	0.0	-22	-0.8	357	0.2	796
239	1012	-77	404	1.4	233	-7	0.0	-44	-1.7	341	0.3	850
300	1502	-137	931	7.6	410	-15	0.1	-64	-2.2	598	0.4	1729
379	1954	-215	908	1.8	611	-47	0.1	-92	-4.3	570	0.8	1733
468	2498	-321	845	-2.0	1003	-62	0.1	-117	-5.4	530	1.0	1871

CB23	alk.	OH^-	Cl^-	SO_4^{2-}	HCO_3^-	Ca^{2+}	Fe^{3+}	K^+	Mg^{2+}	Na^+	charge	Si
days	mmole	mmole	mmole	mmole	mmole	mmole	mmole	mmole	mmole	mmole	meq/L	mmole
0	0.0	0.0	0.0	0.0	0.0	0.0	0.0	0.0	0.0	0.0	0	0.00
95	8.3	-1.0	12.6	0.0	0.6	0.0	0.0	-0.6	0.0	15.5	3	0.01
239	16.9	-4.5	11.4	0.0	3.9	-0.2	0.0	-1.1	-0.1	14.8	2	0.01
300	25.0	-8.1	26.2	0.1	6.8	-0.4	0.0	-1.6	-0.1	26.0	-2	0.01
379	32.6	-12.6	25.6	0.0	10.2	-1.2	0.0	-2.4	-0.2	24.8	-3	0.03
468	41.6	-18.9	23.8	0.0	16.7	-1.5	0.0	-3.0	-0.2	23.0	-5	0.03

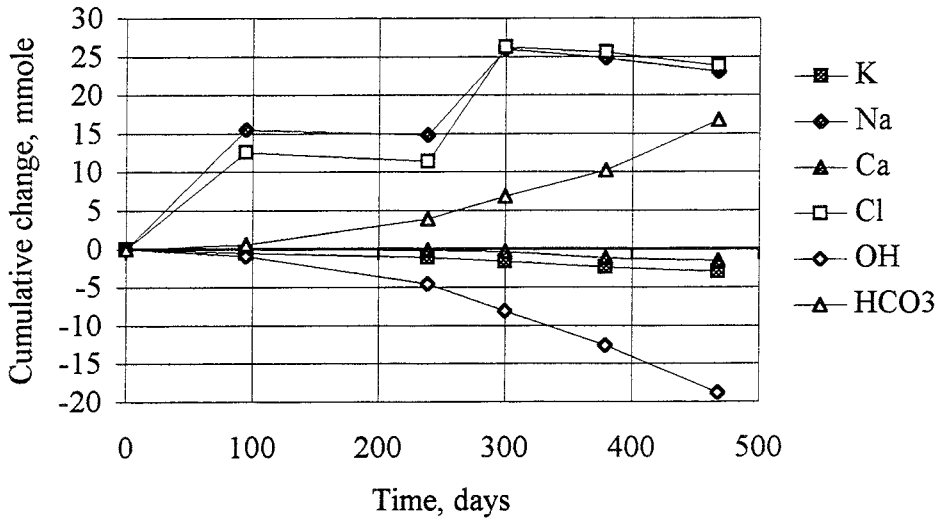

Figure 3-10. *Approximate cumulative changes of total ion content in solutions surrounding sample CB23. Calculated from five successive water analyses.*

Table 3-3. Approximate cumulative changes of total ion content in solutions surrounding sample CB27. Calculated from the five successive water analyses.

CB27	alk.	OH^-	Cl^-	SO_4^{2-}	HCO_3^-	Ca^{2+}	Fe^{3+}	K^+	Mg^{2+}	Na^+	Si	mg
days	mg	mg	mg	mg	mg	mg	mg	mg	mg	mg	mg	total
0	-1	0	0	0	0	0	0.0	0	0	0	0	0
95	2610	-252	357	-2	470	-12	0.0	-376	-1	248	0	433
239	4818	-680	314	11	1158	-28	0.0	-887	-4	215	5	105
300	7331	-1188	751	18	2434	-34	0.0	-1213	-5	494	6	1263
379	10061	-1608	758	37	3615	-115	0.0	-1440	-14	624	66	1923
468	12569	-2249	485	18	5355	-164	0.0	-1780	-21	477	70	2191

CB27	alk.	OH^-	Cl^-	SO_4^{2-}	HCO_3^-	Ca^{2+}	Fe^{3+}	K^+	Mg^{2+}	Na^+	Si	mg
days	mmole	mmole	mmole	mmole	mmole	mmole	mmole	mmole	mmole	mmole	meq/L	mmole
0	0.0	0.0	0.0	0.0	0.0	0.0	0.0	0.0	0.0	0.0	0	0.00
95	43.5	-14.8	10.1	0.0	7.8	-0.3	0.0	-9.6	0.0	10.8	-3	0.01
239	80.3	-40.0	8.8	0.1	19.3	-0.7	0.0	-22.7	-0.2	9.3	-4	0.19
300	122.2	-69.9	21.1	0.2	40.6	-0.9	0.0	-31.1	-0.2	21.5	-4	0.22
379	167.7	-94.6	21.3	0.4	60.3	-2.9	0.0	-36.9	-0.6	27.1	-5	2.36
468	209.5	-132.3	13.6	0.2	89.3	-4.1	0.0	-45.6	-0.9	20.7	-6	2.49

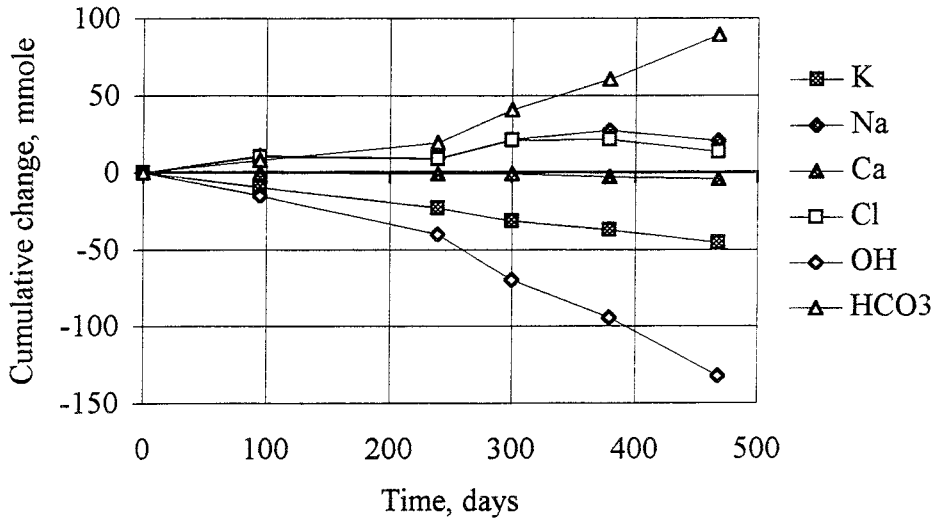

Figure 3-11. *Approximate cumulative changes of total ion content in solutions surrounding sample CB27. Calculated from five successive water analyses.*

3.3 MINERALOGICAL ANALYSES

3.3.1 Elements

Hydrothermal cell tests

A major increase in calcium was found close to the cast cement (Figure 3-12 and appendix C). The content dropped rapidly with increasing distance from the cement but the content was generally higher than in the reference sample. The increase indicates precipitation of calcium-rich secondary minerals since the increase is to large to be explained by ion exchange in the clay or by cement pore water in the clay voids. A small increase of potassium and a decrease of sodium content were significant in all sections. The minor decrease in silicon content in the section close to the cement and the slight increase in the other sections are probably not significant, but related to changes in the content of other elements.

Percolation and diffusion tests

The Figures 3-12 to 3-17 show the distribution of major cations in all analyzed test samples. Reference values refer to the original test material (Table 1-3). A slight increase of calcium was noticed in all percolation and diffusion samples. A minor profile with higher values close to the "cement side" was found in the percolation samples (CB23 and CB27). The content was generally higher in sample CB23, which was an effect of the very high content of potassium in sample CB27. The minor increase of iron in all samples has to be considered as an artifact since the only source for an iron increase was the confining steel construction. The potassium content was generally higher in the test samples than in the reference sample and much higher in the samples percolated by SULF solution. A minor decrease in Si/Al ratio was found in section A in all samples, and a significant general decrease was found in sample CB27. Since no aluminum source was available, a relatively large amount of the original silica content must have been removed from the sample.

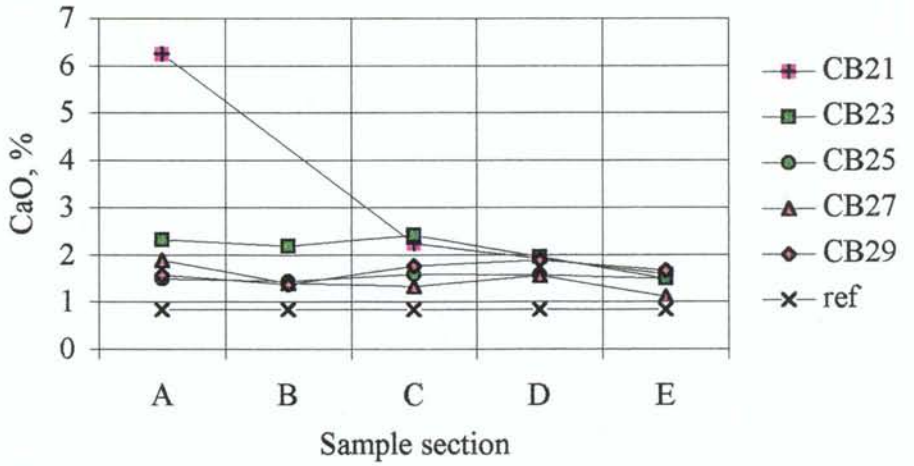

Figure 3-12. *Calcium content distribution in all samples. Section A represent the "cement" side of the samples.*

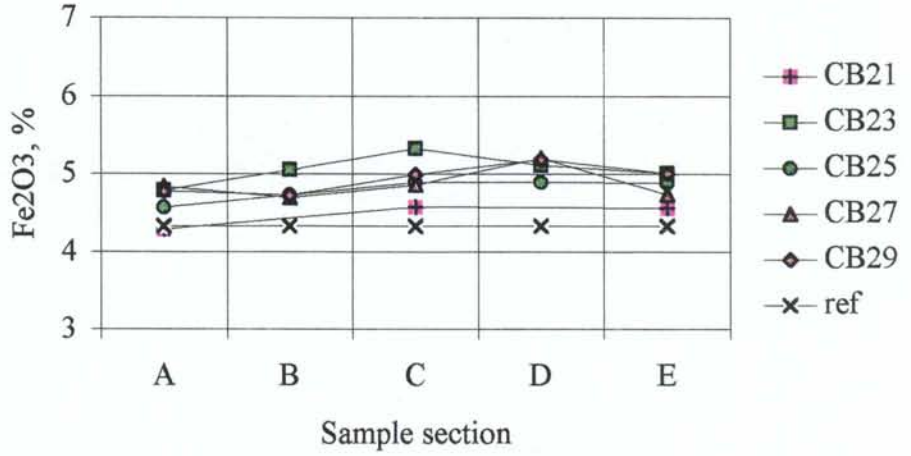

Figure 3-13. *Iron distribution in all samples. Section A represent the "cement" side of the samples.*

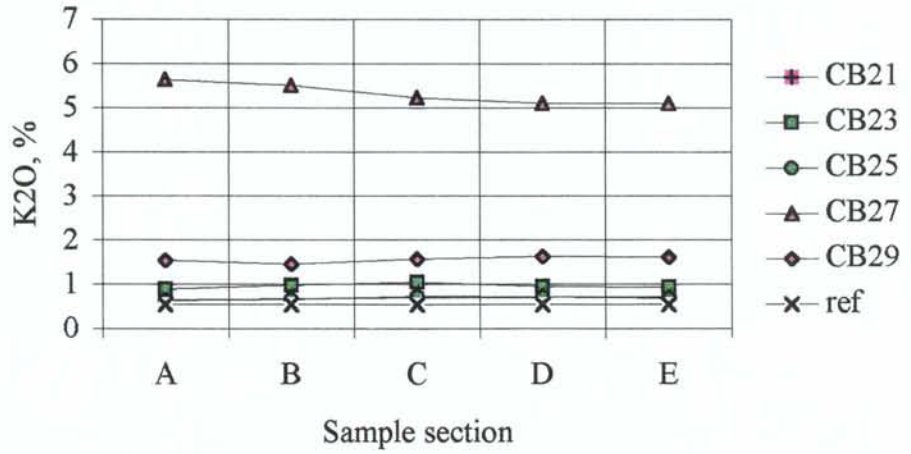

Figure 3-14. *Potassium distribution in all samples. Section A represents the "cement" side of the samples.*

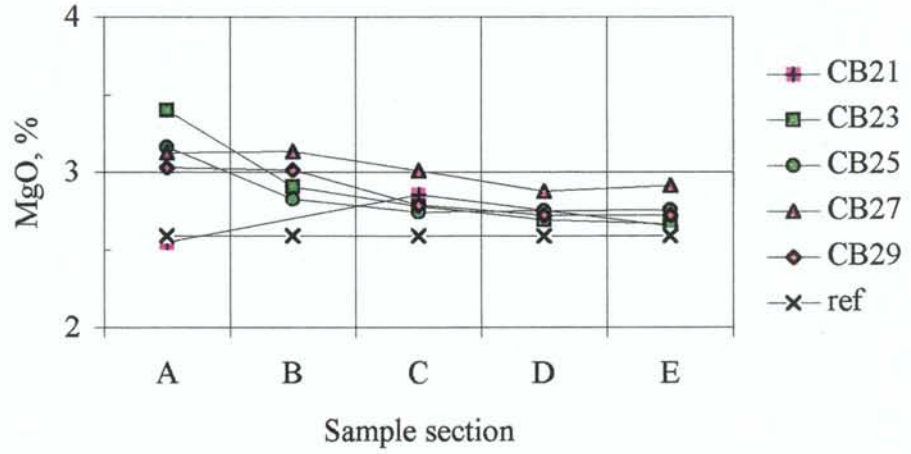

Figure 3-15. *Magnesium distribution in all samples. Section A represents the "cement" side of the samples.*

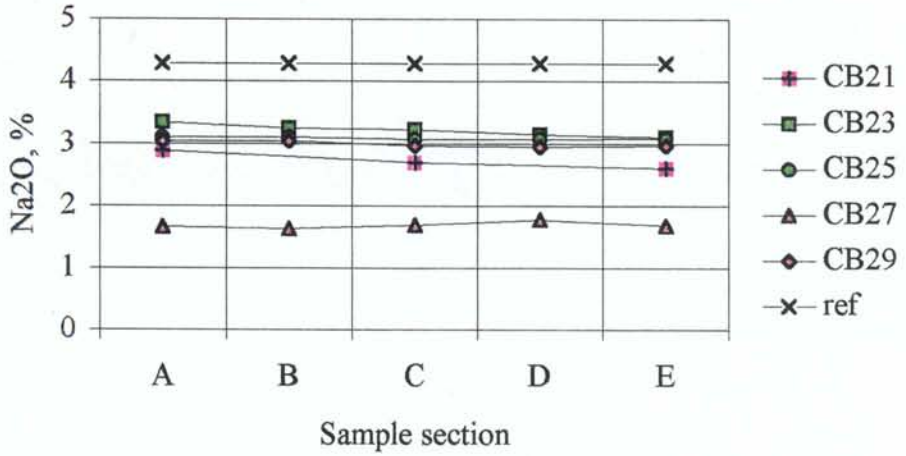

Figure 3-16. *Sodium distribution in all samples. Section A represents the "cement" side of the samples.*

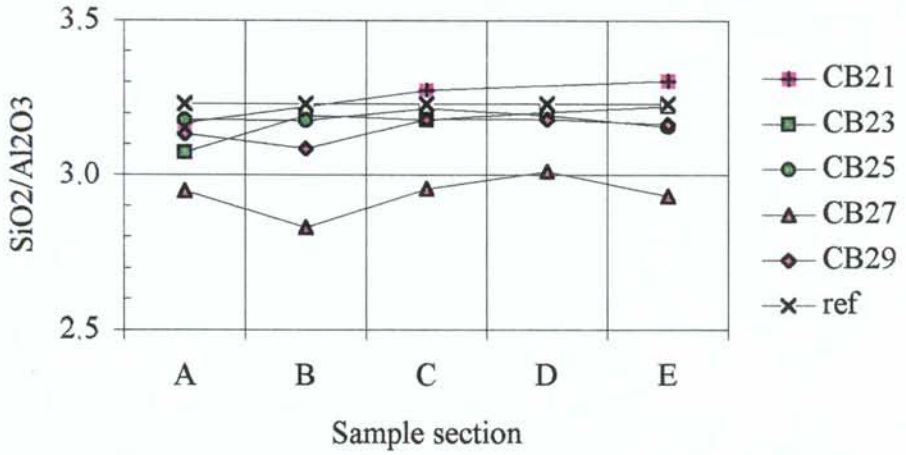

Figure 3-17. *Showing the ratio between SiO_2 and Al_2O_3 in all samples. Section A represents the "cement" side of the samples.*

3.3.2 Cation exchange capacity (CEC)

The CEC values and exchanged ions are shown in Appendix D and in Figure 3-18 to 3-22. The NH_4^+ results shown in the diagrams are equivalent to the CEC values of the actual sample section. The Na^+, Ca^{2+} and K^+ figures represents the exchanged original cations and the sum of these are shown as SEC (Sum of Exchanged Cations).

A minor CEC increase and a marked ion exchange from Na^+ to Ca^+ compared to the reference sample were found in all sections in sample CB21 (Figure 3-18). The SEC and the CEC values were similar in the two sections closest to the cast cement but excess Ca^{2+} was exchanged in the outer section. The samples CB23 and CB25, which were contacted to AWP solution, were dominated by Na^+ in exchange position and only a minor increase in K^+ content was noticed. A significant increase in CEC was found

in both samples, especially at the NASK solution side of sample CB25. In the samples contacted to SULF solution an ion exchange from Na^+ to K^+ was obvious in all sections. The CEC values from the percolated sample CB27 were close to that of the reference material, and to the SEC values, throughout the sample. This was not the case in the diffusion test sample CB29 in which the CEC values were significantly increased and poorly correlated to the SEC values. The highest cation exchange capacities in this test series were consequently found in the diffusion tests, were poorly correlated to the SEC values and were located at the low concentration side of the samples with respect to the cement solutions.

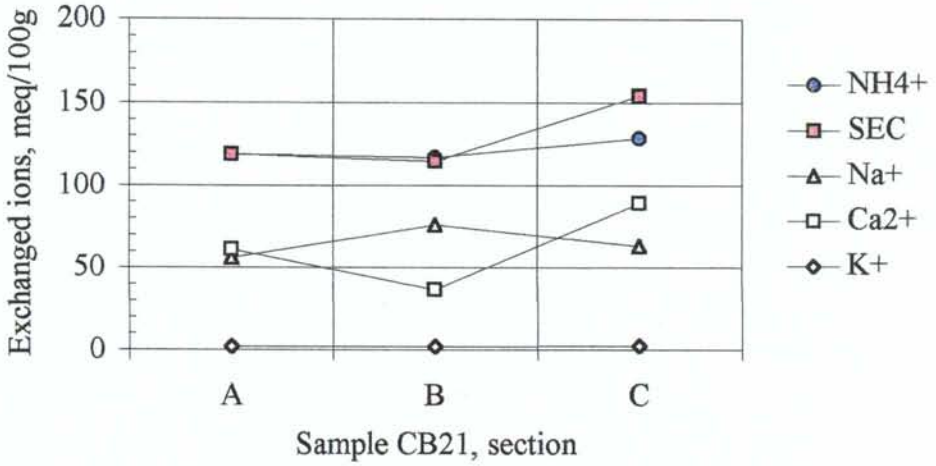

Figure 3-18. *Exchanged cations from the clay fraction in 3 sections in sample CB21. Section A represents the "cement" side of the samples. The NH_4^+ results are equivalent to the CEC values, SEC represent the Sum of Extracted Cations, and Na^+, Ca^{2+} and K^+ are the analyzed extracted cations.*

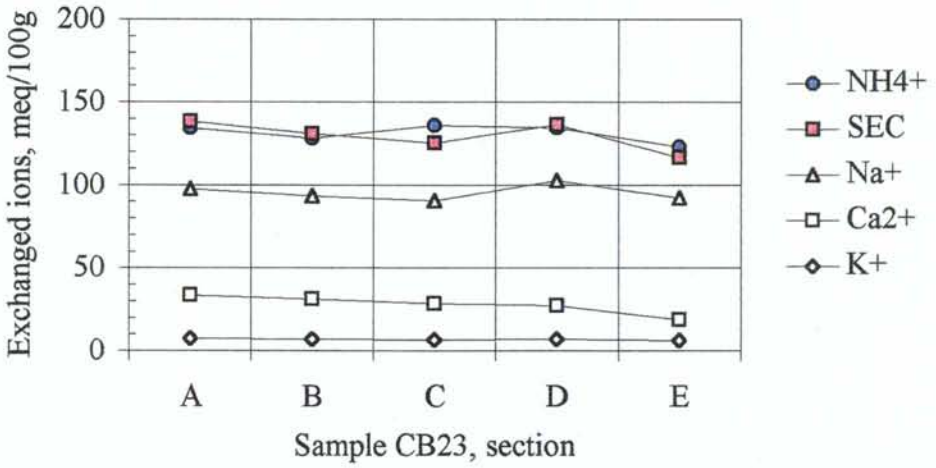

Figure 3-19. *Exchanged cations from the clay fraction in 5 sections in sample CB23. Section A represents the "cement" side of the samples. The NH_4^+ results are equivalent to the CEC values, SEC represent the Sum of Extracted Cations, and Na^+, Ca^{2+} and K^+ are the analyzed extracted cations.*

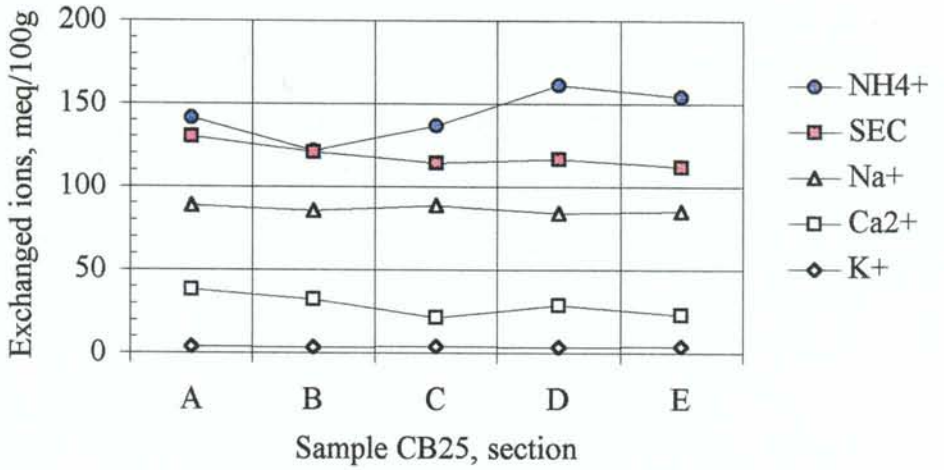

Figure 3-20. *Exchanged cations from the clay fraction in 5 sections in sample CB25. Section A represents the "cement" side of the samples. The NH_4^+ results are equivalent to the CEC values, SEC represent the Sum of Extracted Cations, and Na^+, Ca^{2+} and K^+ are the analyzed extracted cations.*

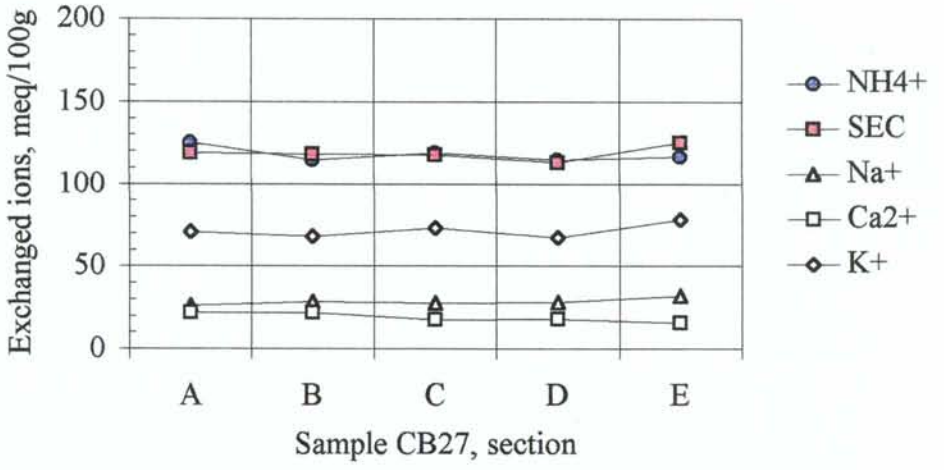

Figure 3-21. *Exchanged cations from the clay fraction in 5 sections in sample CB27. Section A represents the "cement" side of the samples. The NH_4^+ results are equivalent to the CEC values, SEC represent the Sum of Extracted Cations, and Na^+, Ca^{2+} and K^+ are the analyzed extracted cations.*

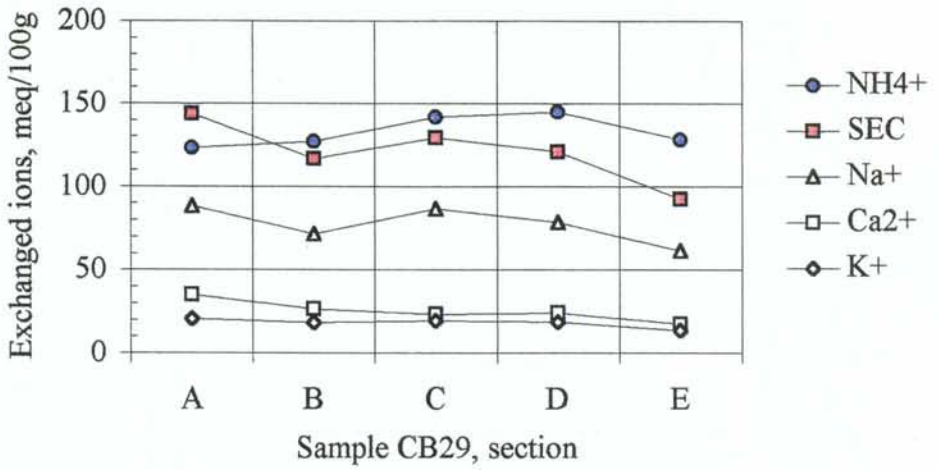

Figure 3-22. *Exchanged cations from the clay fraction in 5 sections in sample CB29. Section A represents the "cement" side of the samples. The NH_4^+ results are equivalent to the CEC values, SEC represent the Sum of Extracted Cations, and Na^+, Ca^{2+} and K^+ are the analyzed extracted cations.*

3.3.3 X-ray diffraction (XRD)

A detailed account of the analyses is given in Appendix A, in which the diffractometer patterns of the analyzed sections in one sample are superimposed on the pattern of the reference sample. Expected reflections from possible minerals are shown as vertical bars below the x-axis in order to facilitate the mineral identification. The length of the bars show the probable relative intensities for the different peaks related to certain mineral.

No major differences were found between the various sections within the samples nor between the different analyzed samples, including the reference sample. (Figure 3-23). However, a number of minor but significant mineral alterations were detected. The following observations and comparisons with reference material were generally applicable to the analyzed specimens:

- no sign of typical zeolite related peak patterns,
- no systematic area increase of feldspar related peaks,
- no area increase of calcite related peaks,
- appearance of "broad peaks" (or rather hills) indicating calcium silicate hydrates, possibly CSH(I).
- area increase of quartz related peaks,
- area decrease of cristobalite related peaks,
- area increase of peaks probably related to illite and chlorite.

Most zeolites give a complicated and typical XRD pattern and are therefore easy to detect. It is therefore likely that no zeolites were present in the analyzed specimens, although it can not be excluded that extremely fined grained crystals may stay undetected. The natural variation in feldspars composition and content make the interpretation difficult. A minor K-

feldspar formation in the samples exposed to the SULF solution may possibly have taken place. Most analyzed specimens had a peak area increase at 29.3° (2θ) which is the typical position for the main calcite peak. Unfortunately, this is also the position of a major CSH(I) peak. The interpretation that the observed reflections mainly are due to a CSH mineral is based on the complete expected patterns of the two possible minerals. XRD patterns from quartz are generally very significant but the natural uneven distribution in the original MX-80 material makes the interpretation uncertain. However, the quartz peak areas systematically increase from the high concentration side of the samples to the low concentration side, and the peak areas are larger in all 15 analyzed specimens exposed to high pH compared to the reference sample, which support the conclusion that quartz was formed during the tests. Cristobalite may be identified from two peaks located at 21.9° and 36.1° (2θ). The latter one is concealed in clay related peaks and the former peak may be mixed up with plagioclase feldspar. The interpretation that the peak at 21.9° (2θ) represent cristobalite is based on the peak broadness, which reflects the poor crystallinity, and on the fact that the peak disappearance is not accompanied by a decrease in other plagioclase feldspar related peaks.

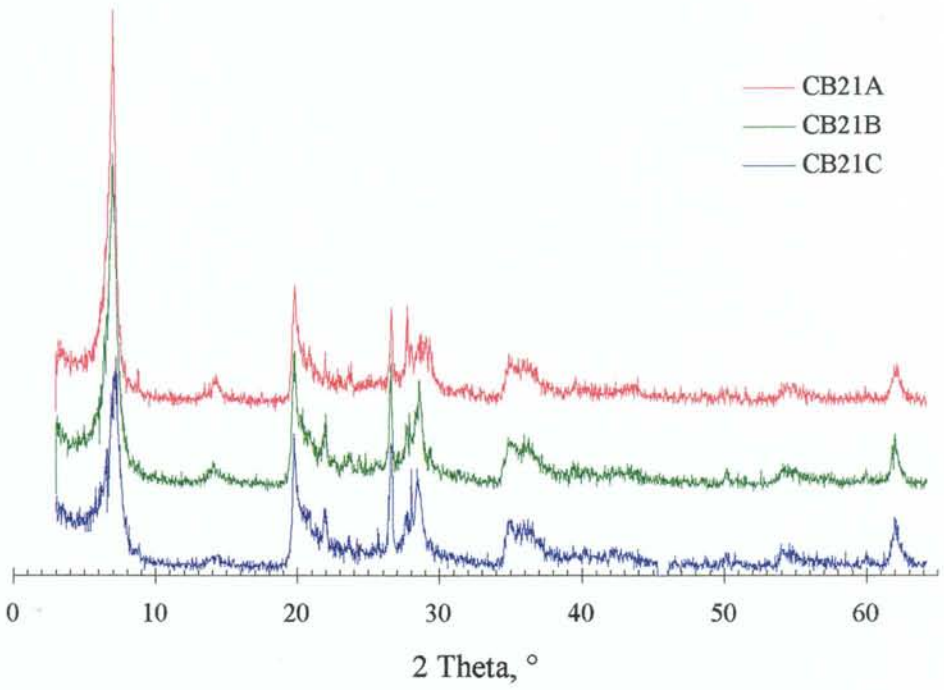

Figure 3-23. *XRD diagram of sample CB21 showing the relatively similar patterns from the three analyzed sections.*

The changes in the sample contacted to cast cement (CB21) were generally smaller than the changes in the samples contacted to cement solutions. A pronounced "change gradient" with respect to cristobalite dissolution, quartz increase, and CSH neoformation was found (Figure 3-24). The largest changes were logically found in the section nearest to the cast cement. In the sample percolated by SULF solution a significant neoformation of probably illite and possibly also of chlorite (Figure 3-25). The peaks probably related

to the chlorite were small but the fact that they were found in all three analyzed sections support the conclusion. The same tendency, with increased peaks related to illite and chlorite, was found also in the other samples contacted to cement solution, although weaker.

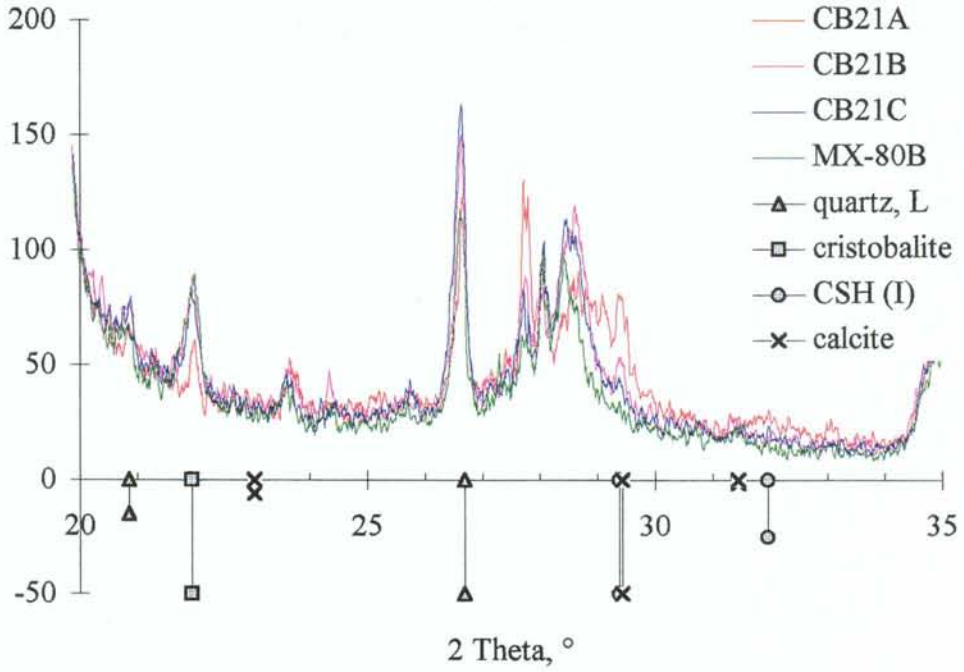

Figure 3-24. *Part of diffraction patterns of sample CB21 showing the relatively large changes in section A compared to reference sample (MX-80B) and the smaller changes in section B and C.*

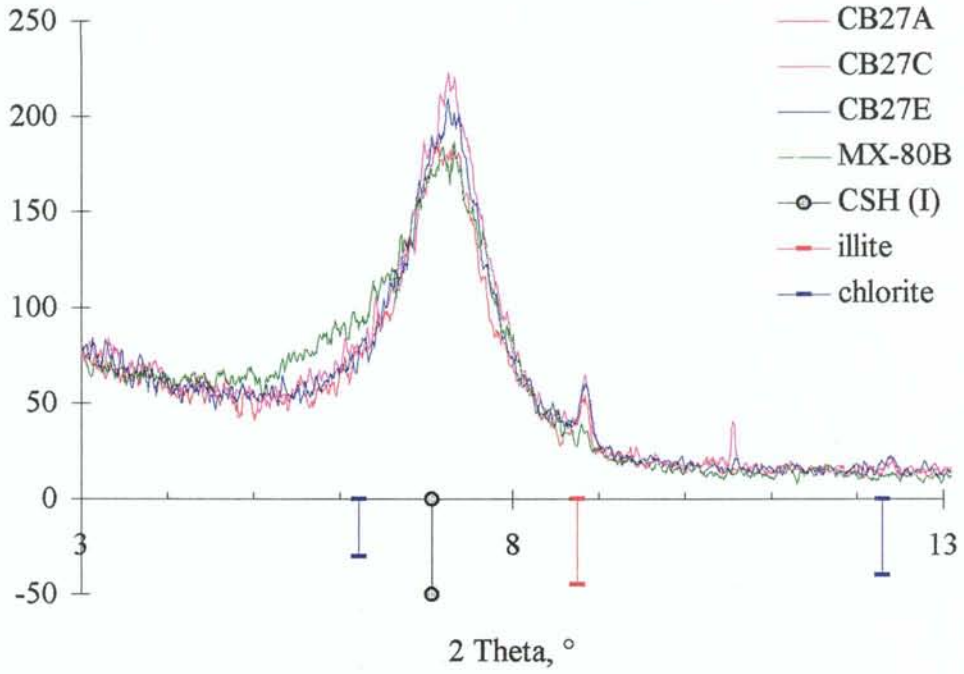

Figure 3-25. *Part of diffraction patterns of sample CB27 showing the increase of peaks related to illite and chlorite.*

3.3.4 Scanning electron microscopy (SEM-EDX)

Analyses were made on different parts of the various clay samples but also of solid material which was filtered from the NASK solutions. The surveying study of the clay samples clearly showed that the major mass had a montmorillonitic appearance and composition. The EDX micro-analyses supported the results which were found in the ICP-AES clay sample analyses, CEC analyses and the XRD analyses. The general increase of potassium in sample CB27 and CB29 was evenly distributed and mainly related to the clay structure. The general increase of calcium was found in all samples and it was often related to non-clay structures except in sample CB27. Figure 3-26 (3819) shows a frequently found precipitation of micron-sized granules which were incorporated in the clay structure. The granule composition was dominated by silicon and calcium in varying ratios, and occasionally with aluminum as minor component. These silicon-calcium structures were rare in sample CB27, however, the composition of the filtrate from NASK solution at the low pressure side was dominated by silicon and with approximately equal amounts of calcium, magnesium and potassium as secondary minerals (Figure 3-27, 3795). In a few cases an erionite-like (zeolite) structure was found in the filtrate but the content of aluminum was lower than normally found in this mineral (Figure 3-28, 3799). Large grains of feldspars were infrequently found in all samples. The grains normally had a typical morphology (Figure 3-29, 3821), but grains which seemed to be etched were found as well (Figure 3-30, 3802). No significant tendency was consequently found concerning neoformation-dissolution processes. Fibrous structures with a typical clay composition and relatively high content of potassium were occasionally found. The finding support the results from XRD analyses concerning illite formation. The fibrous character and the location in probable pores indicate that the mineral was neoformed from a solution, and not formed by collapsed montmorillonite (Figure 3-31, 3812 and Figure 3-32, 3801).

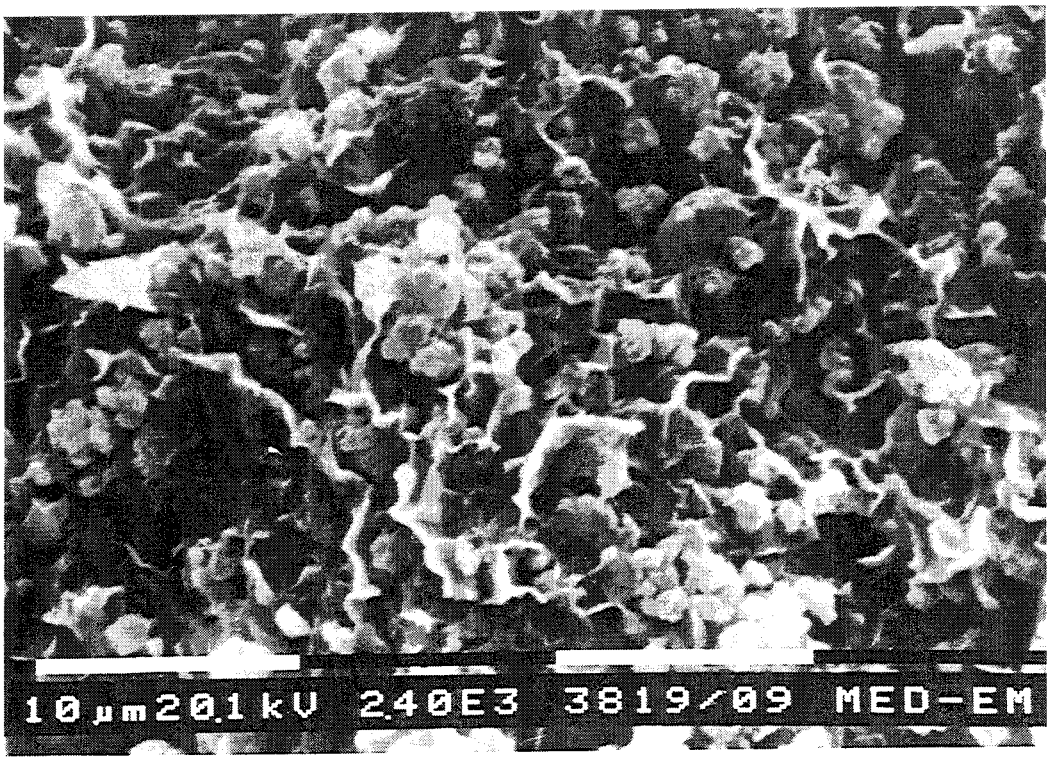

Figure 3-26. *Precipitation in sample CB23. The granule composition was dominated by silicon and calcium in varying ratios, and occasionally with aluminum as minor component (3819).*

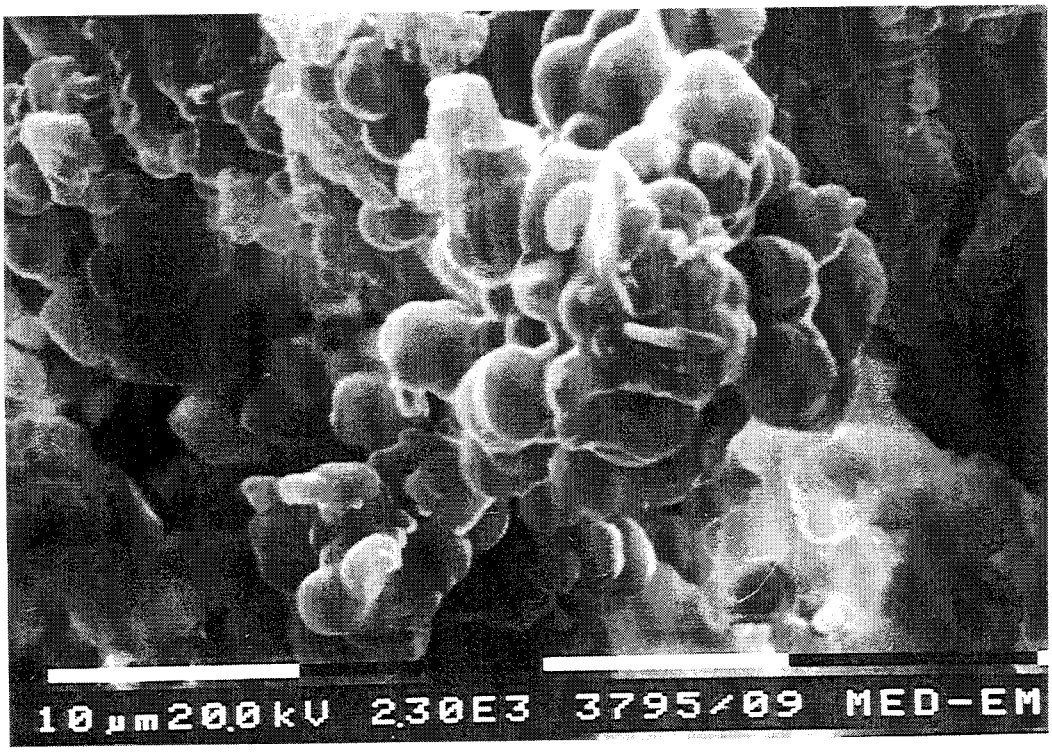

Figure 3-27. *Filtrate from NASK solution at the low pressure side of sample CB27. The material was dominated by silicon (~50%) and with approximately equal amounts of calcium, magnesium and potassium as secondary elements (3795).*

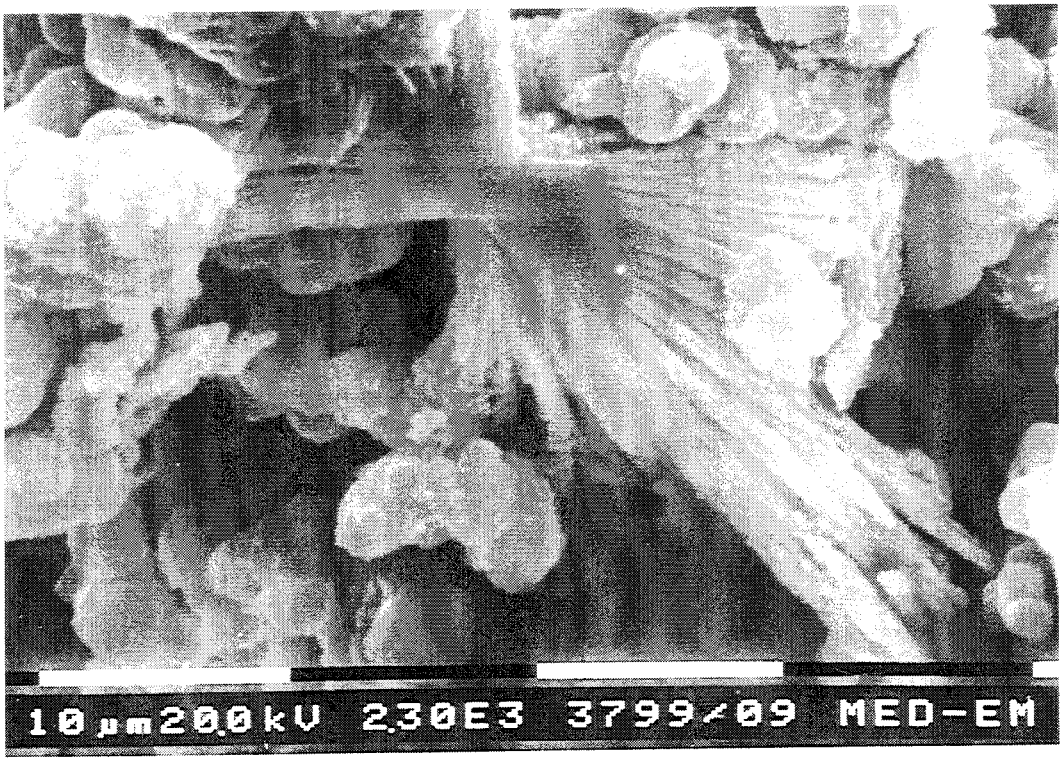

Figure 3-28. *Erionite-like (zeolite) structure found in the NASK solution at the low pressure side of sample CB27. The element composition was typical for this mineral with the exception for a low aluminum content (3799).*

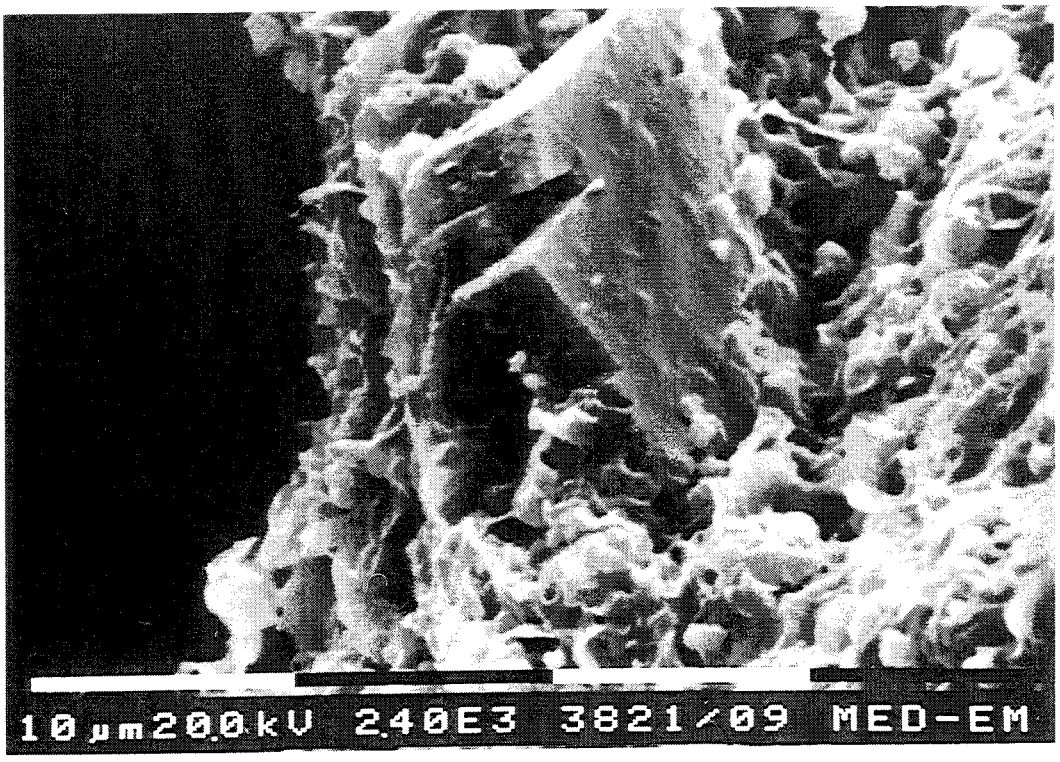

Figure 3-29. *Large plagioclase feldspar grain from samples CB23 (3821).*

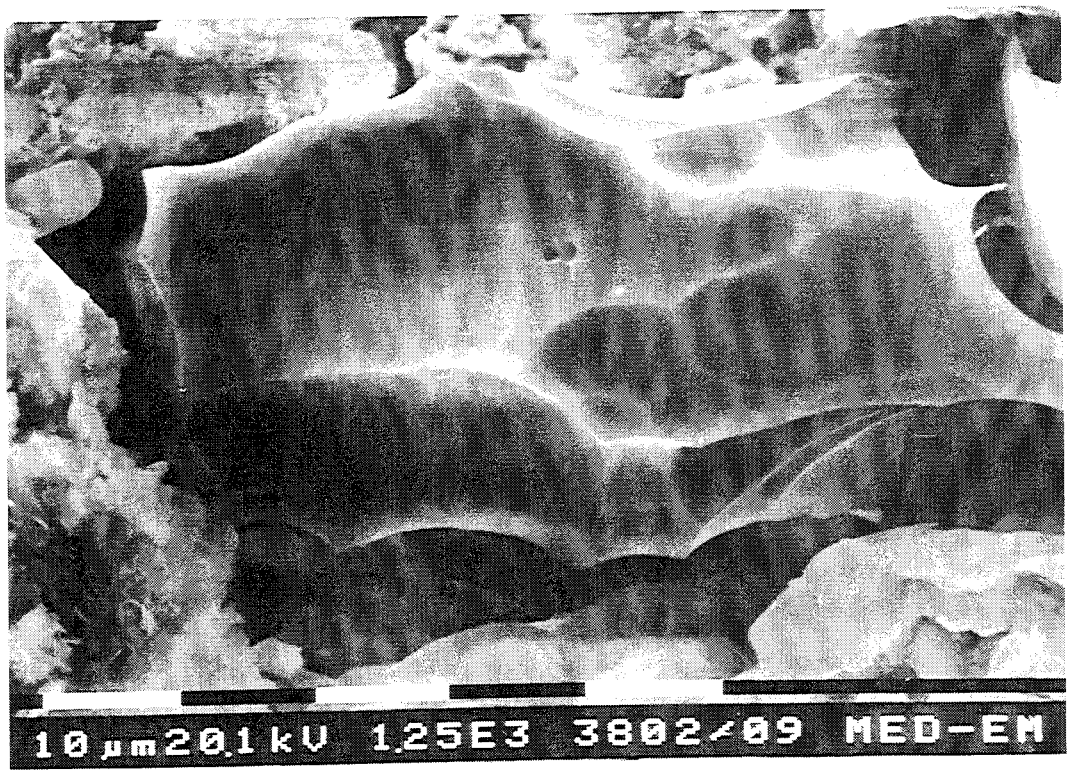

Figure 3-30. *Probably etched grain found in samples CB27. The element composition indicate that the mineral is potassium feldspar. (3802).*

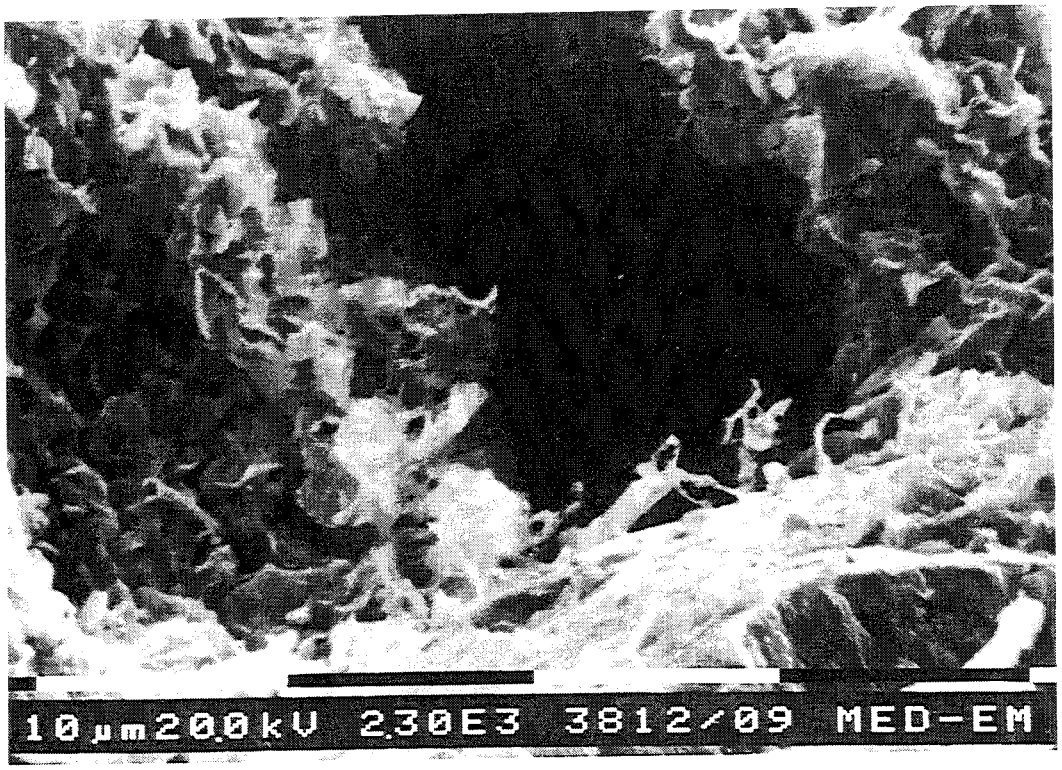

Figure 3-31. *Fibrous and potassium rich clay, probably illite, growing into pores in sample CB23 (3812).*

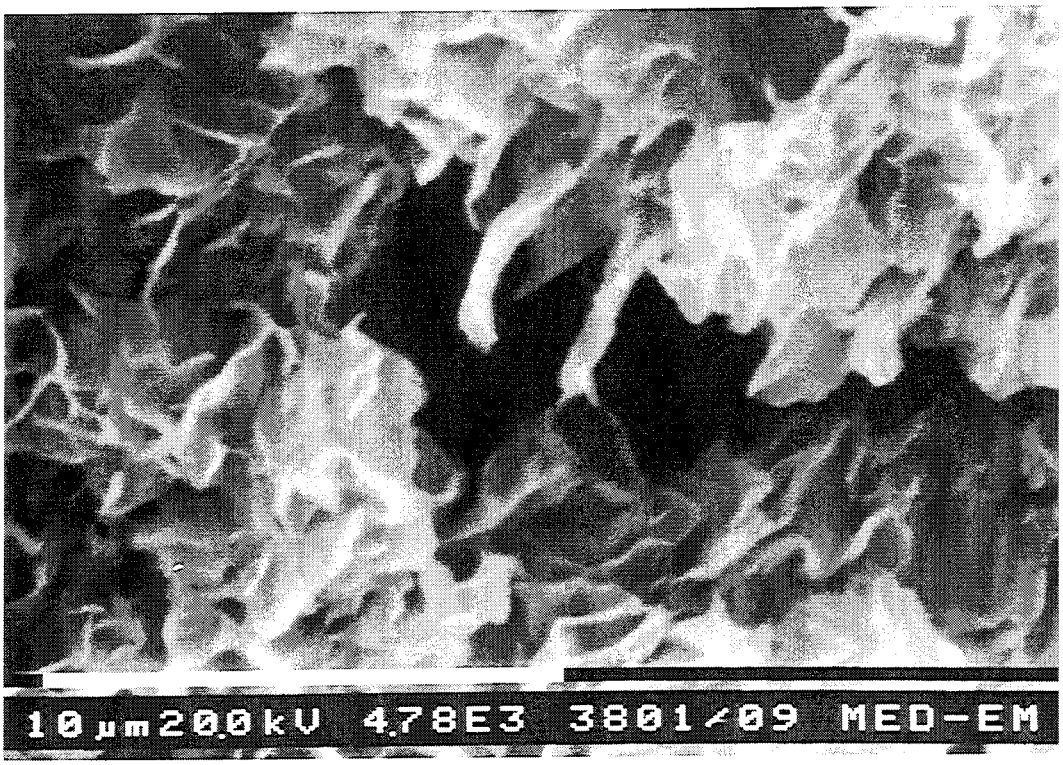

Figure 3-32. *Thin ribbons of filamentous potassium rich clay, probably illite, growing into pores in sample CB27 (3801).*

4 CONCLUSIONS AND DISCUSSION

Geochemical modeling of cement in contact with bentonite have predicted dissolution of the montmorillonite in bentonite and neoformation of K-feldspar and Ca-zeolites, partly as a consequence of the high pH. The present results do not show clear evidence of such neoformation. However, minor other mineralogical alteration processes have been found in the bentonite. The test results from the present study give a fairly unanimous qualitative picture of the mineralogical changes which were largest in the samples percolated by the SULF solution, but significant also in the samples contacted to pore-water from ordinary Portland cement. The most important findings may be summarized in the following items:

- Dissolution of original cristobalite.
  The dissolution was complete in all sections in the samples contacted to the SULF solution (CB27 and CB29). The dissolution was larger at the high concentration side in the samples contacted to AWP solution (CB23 and CB25). Dissolution was only found in the section close to the cast cement in the cement -bentonite contact test (CB21).

- Increase in quartz content.
  Increase was found in all sections in all samples, and generally with more quartz at the low concentration side of the samples. The final mean quartz content in the samples contacted to cement solutions were several times the original content, while the mean increase was roughly 50% in sample CB21.

- Formation of CHS-gels.
  The CSH material was probably in the form of CSH(I) according to XRD analyses. A meaningful quantification of the neoformation is not possible due to the poor crystallinity of the substance. However, the highest content was found in sample CB27, followed by equal content in sample CB23 and CB29, somewhat less in sample CB25, and finally least in sample CB21. In the latter sample the content was high in the section close to the cast cement but only indicated in the other two sections.

- Minor formation of illite and chlorite.
  The formation was only significant in the percolated samples (CB23 and CB27). The fibrous structure observed by SEM indicate that the illite was neoformation in voids and not formed by collapse of montmorillonite. Comparison of results from the 4 and 16 month tests indicate that the illite and chlorite formation rate seem to be retarding. This may be due to the heterogeneity of the original montmorillonite, which may give a distribution in disposition towards illitization. Alternatively, the formation may be governed by dissolution of other minerals than montmorillonite, e.g. cristobalite. The original content of such a mineral would consequently limit the neoformation

- Silicon was dissolved and transported out of samples CB27:
  Precipitation took place in the artificial rock solution at the low pressure side. The precipitate contained silicon as dominating element and approximately equal contents of calcium, magnesium and potassium as secondary elements. The total loss in the sample was less than 5% of the original mass.

- A minor increase in cation exchange capacity in all samples.
  The two samples which were only contacted to cement solutions had the largest increases, which was located at the low concentration side. A possible explanation is that neoformed substances in these samples caused the increase and that corresponding substances in the percolated samples were transported out of the samples by the percolating water.

- No clear proof of montmorillonite lattice alteration or breakdown was found.

- No significant changes in the content of, or relation between, different kinds of feldspars were found.

The percolated volume of SULF solution in sample CB27 was approximately 10 times the pore volume in the sample. Still, the observed mineralogical changes only concerned a minor part of the bentonite mass, and the effects of these changes on the buffer functions are probably not significant. The measured changes, in swelling pressure and hydraulic conductivity in the percolated samples, were most likely an effect of ion exchange from the original charge balancing cation to the percolating alkali or calcium ions.

REFERENCES

1. Müller-Vonmoos M., Kahr G., 1983. Mineralogiche Untersuchungen von Wyoming Bentonit MX-80 und Montigel. NTB 83-12, Baden.

2. Hjorth J., Skibsted J., Jacobsen H.J., 1988. ^{29}Si MAS NMR studies of Portland cement components and effects of microsilica on the hydration reaction. Cement and concrete research vol. 18, pp. 789-798. Pergamon Press.

3. Karnland O., Pusch R., Sandén T., 1994. The effects of cyclic hydration/dehydration on Na and K bentonites. SKB AR 94-40, Stockholm.

4. Karnland O., Pusch R., Sandén T., 1994. Karakterisering av buffertmaterial. Laboratoriemetoder för bestämning av mineralogiska och fysikaliska egenskaper. SKB AR 94-60, Stockholm.

5. Karnland O. 1995. Salt redistribution and enrichment in compacted bentonite exposed to a thermal gradient. SKB AR 95-31, Stockholm

APPENDICES

A XRD diagrams

A1 3-35° (2θ), sample CB21
A2 35-65° (2θ), sample CB21
A3 20-40° (2θ), sample CB21 feldspar reference indications

A4 3-35° (2θ), sample CB23
A5 35-65° (2θ), sample CB23
A6 20-40° (2θ), sample CB23 feldspar reference indications

A7 3-35° (2θ), sample CB25
A8 35-65° (2θ), sample CB25
A9 20-40° (2θ), sample CB25 feldspar reference indications

A10 3-35° (2θ), sample CB27
A11 35-65° (2θ), sample CB27
A12 20-40° (2θ), sample CB27 feldspar reference indications

A13 3-35° (2θ), sample CB29
A14 35-65° (2θ), sample CB29
A15 20-40° (2θ), sample CB29 feldspar reference indications

B Water analyses

B1 Hydrothermal cell tests
B2 Percolation and diffusion tests. Analyses from 1993-11-01
B3 Percolation and diffusion tests. Analyses from 1994-03-25
B4 Percolation and diffusion tests. Analyses from 1994-05-25
B5 Percolation and diffusion tests. Analyses from 1994-08-12
B6 Percolation and diffusion tests. Analyses from 1994-11-09

C Clay element analyses

D Cation exchange analyses

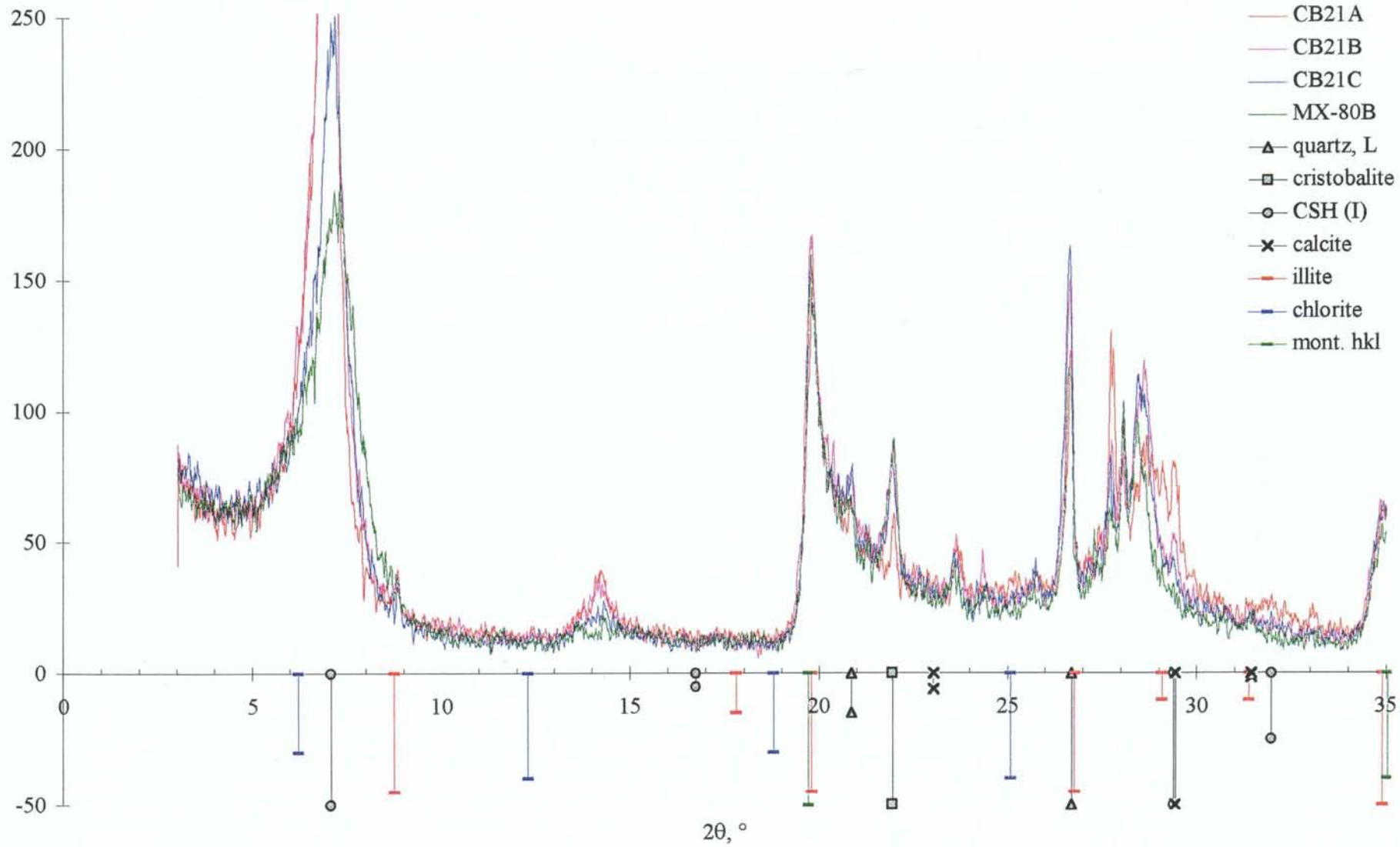
250
200
150
100
50
0
-50
0
5
10
15
20
25
30
35
2θ, °
CB21A
CB21B
CB21C
MX-80B
quartz, L
cristobalite
CSH (I)
calcite
illite
chlorite
mont. hkl

A1

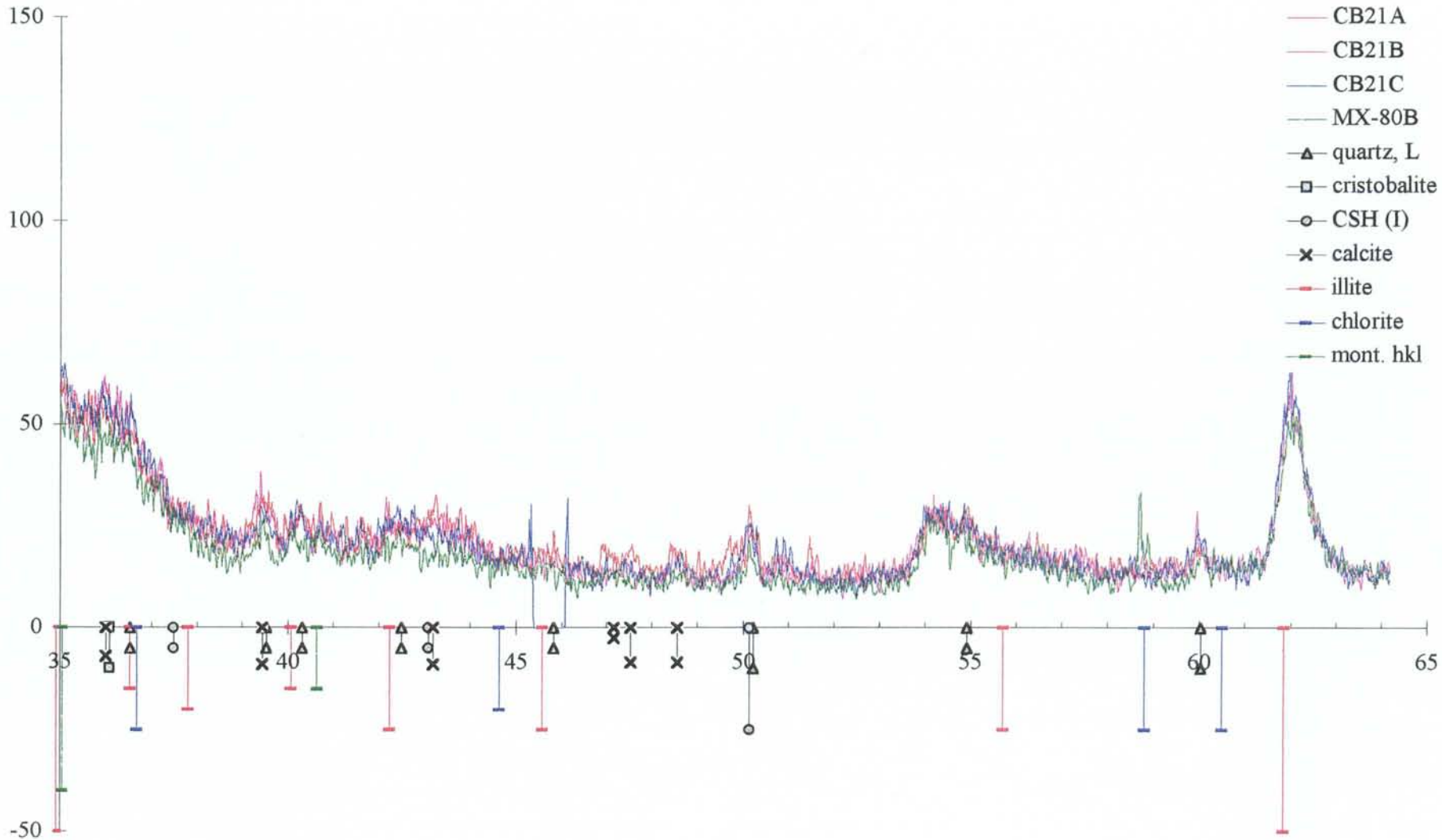
150
100
50
0
-50
35
40
45
50
55
60
65
2θ, °
CB21A
CB21B
CB21C
MX-80B
quartz, L
cristobalite
CSH (I)
calcite
illite
chlorite
mont. hkl

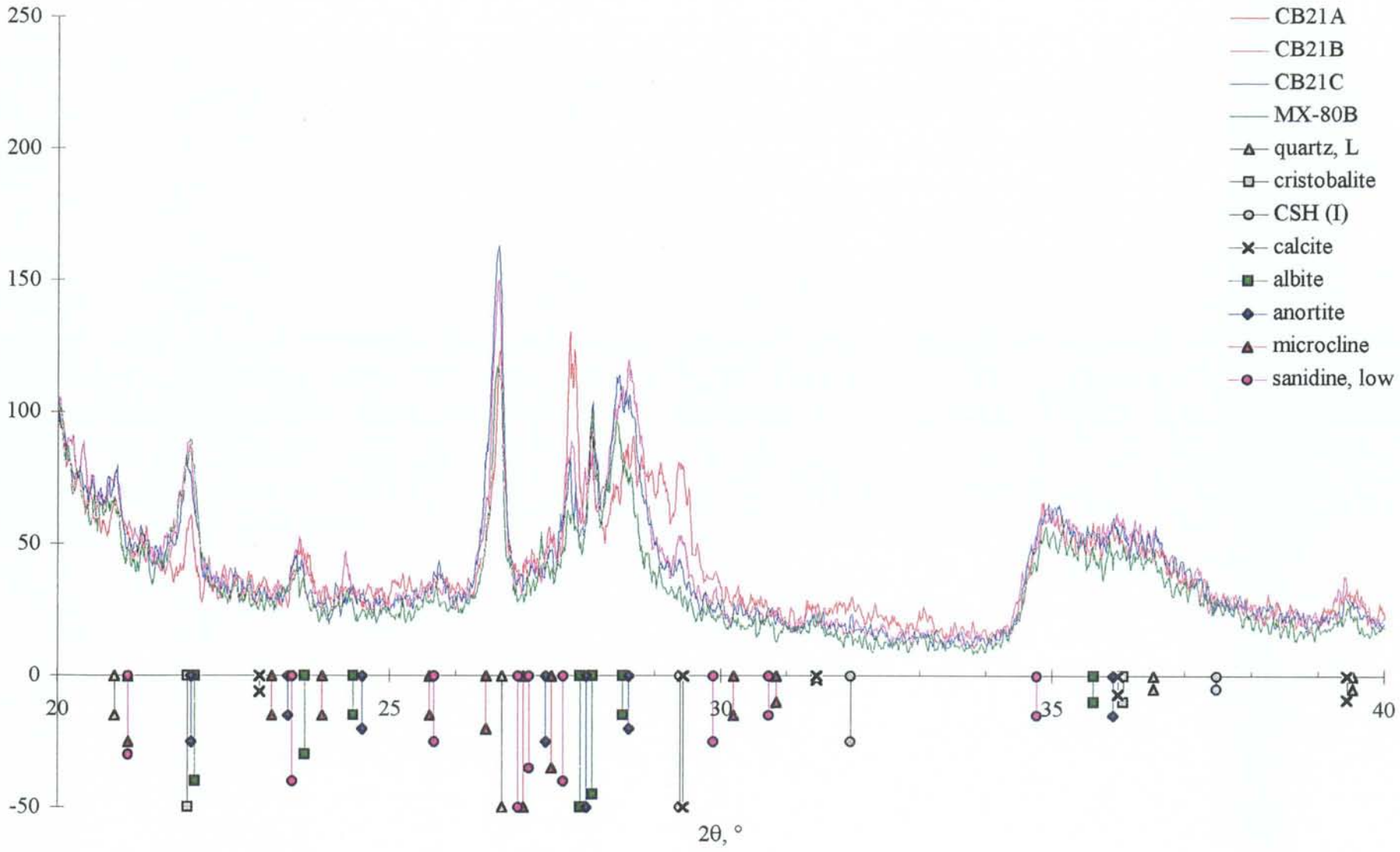
250
200
150
100
50
0
-50
20
25
30
35
40
2θ, °
CB21A
CB21B
CB21C
MX-80B
quartz, L
cristobalite
CSH (I)
calcite
albite
anortite
microcline
sanidine, low

A3

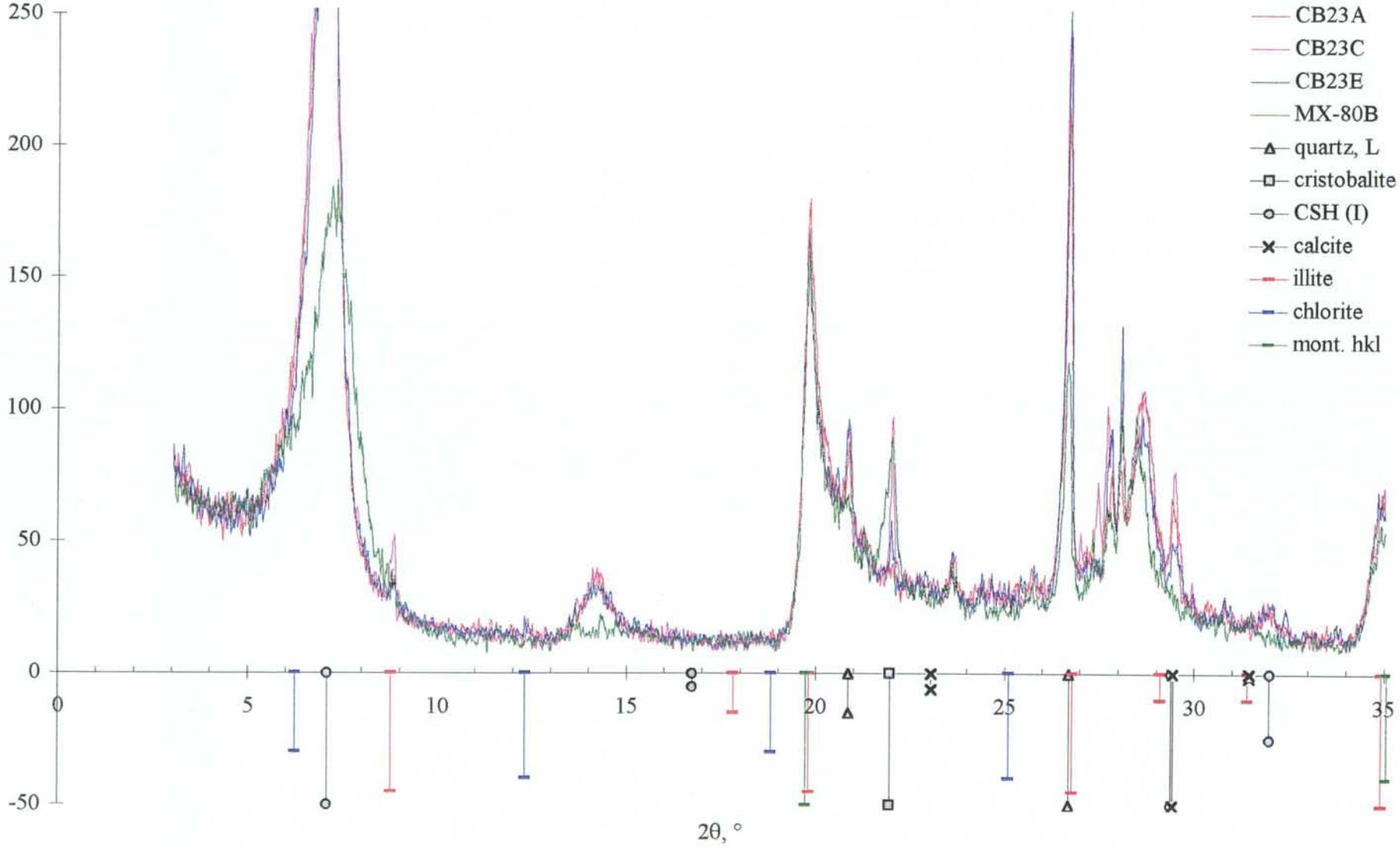
250
200
150
100
50
0
-50
0
5
10
15
20
25
30
35
2θ, °
CB23A
CB23C
CB23E
MX-80B
quartz, L
cristobalite
CSH (I)
calcite
illite
chlorite
mont. hkl

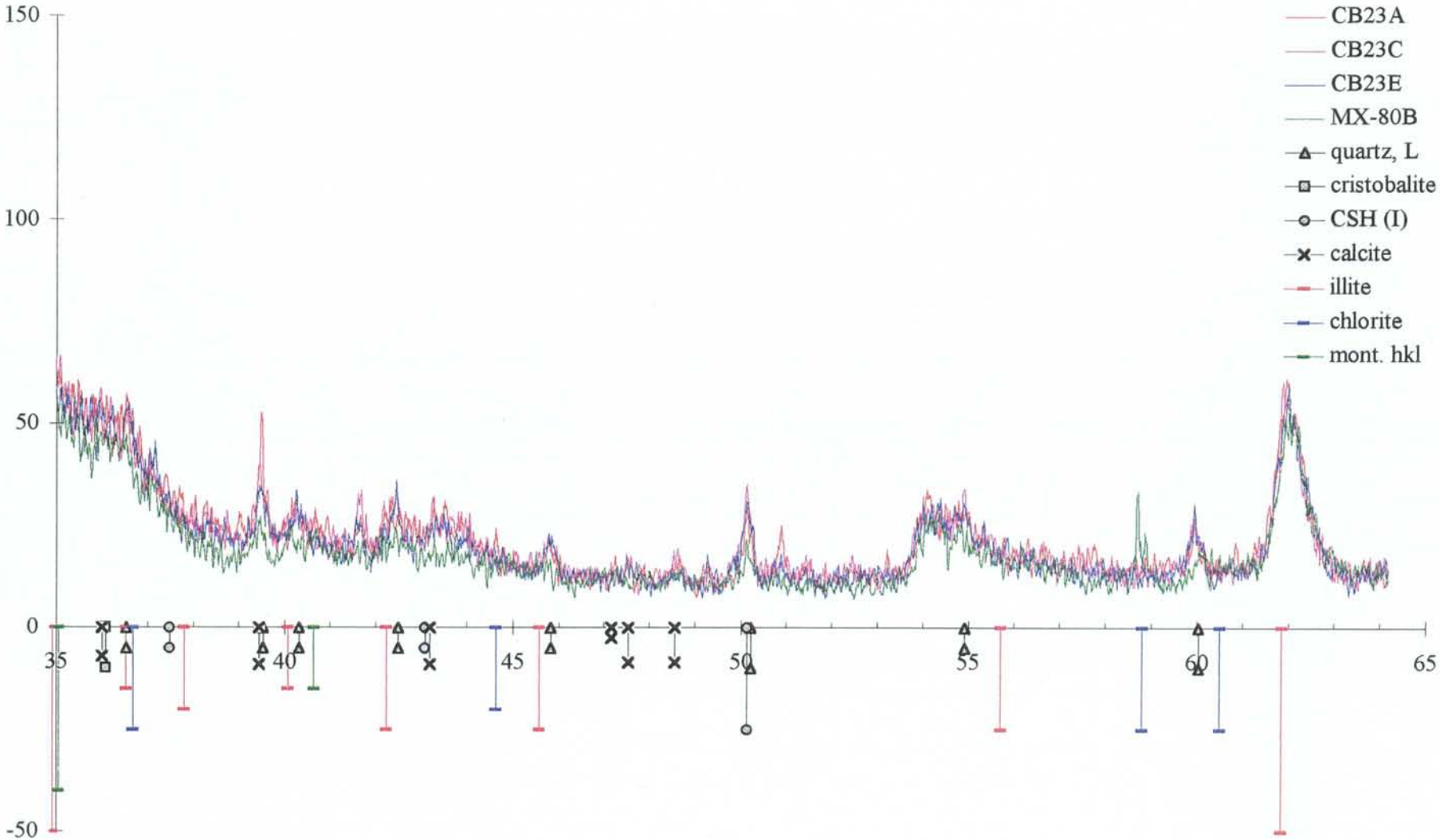
150
100
50
0
-50
35
40
45
50
55
60
65
2θ, °
CB23A
CB23C
CB23E
MX-80B
quartz, L
cristobalite
CSH (I)
calcite
illite
chlorite
mont. hkl

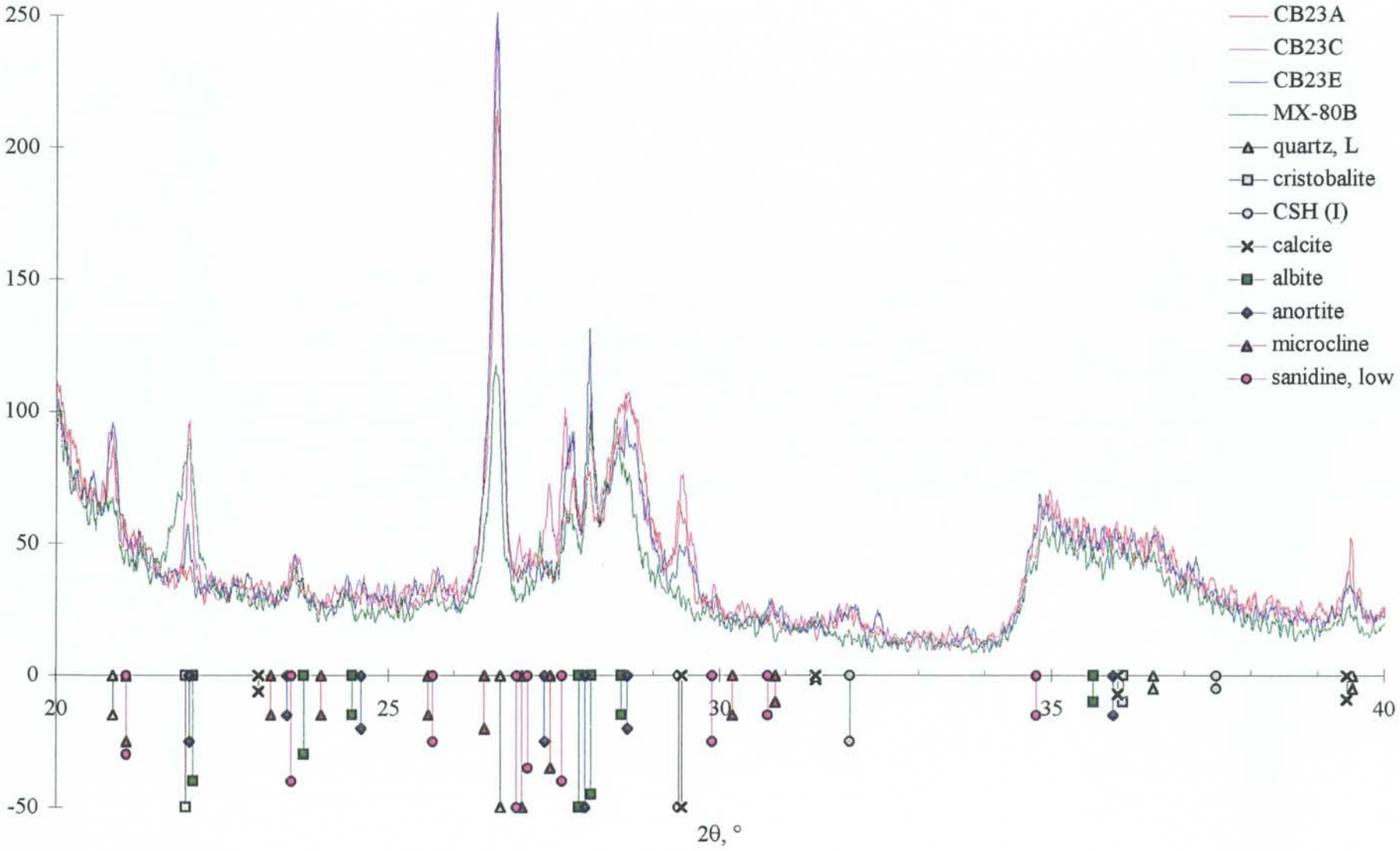
250
200
150
100
50
0
-50
20
25
30
35
40
2θ, °
CB23A
CB23C
CB23E
MX-80B
quartz, L
cristobalite
CSH (I)
calcite
albite
anortite
microcline
sanidine, low

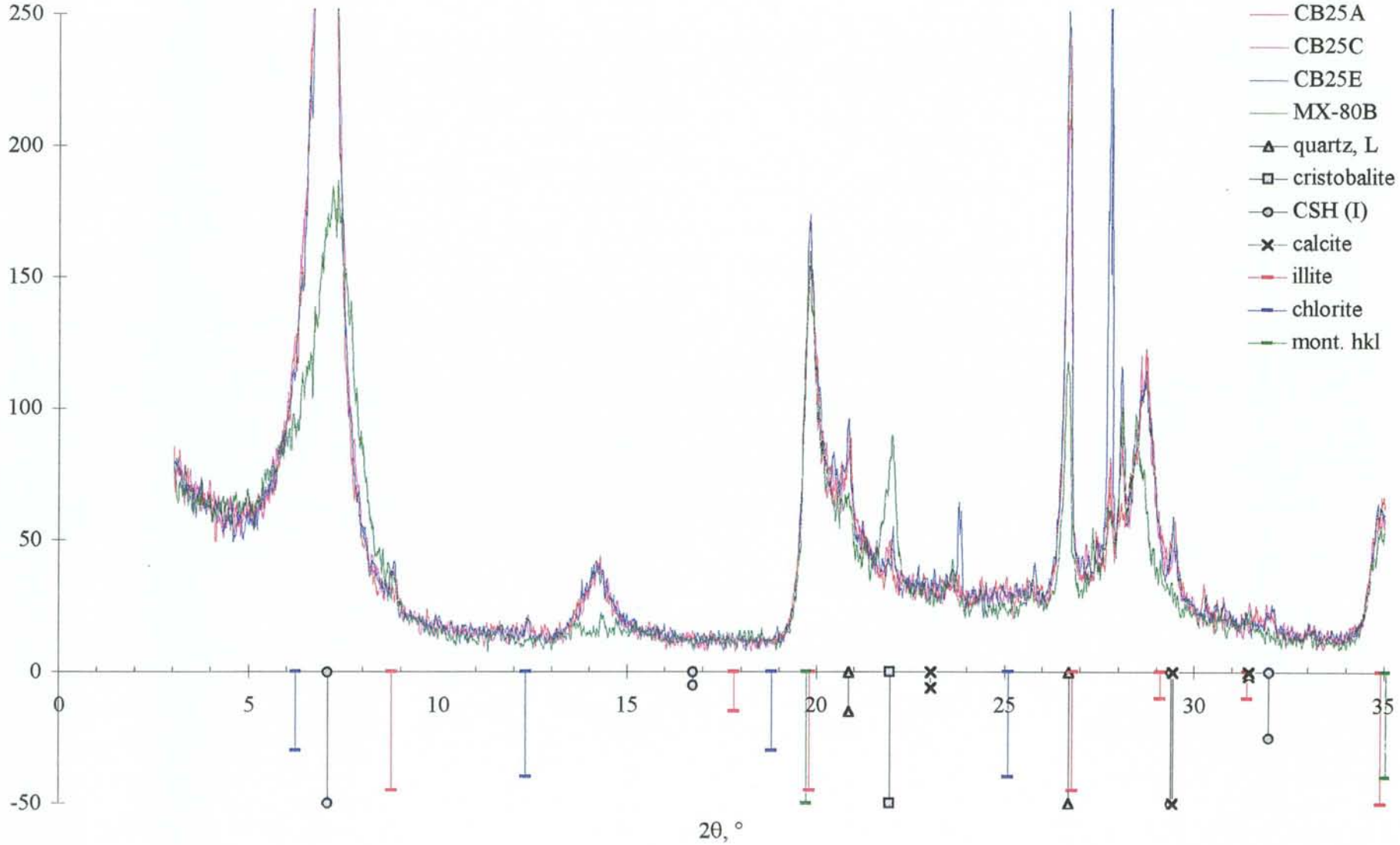
250
200
150
100
50
0
-50
0
5
10
15
20
25
30
35
2θ, °
CB25A
CB25C
CB25E
MX-80B
quartz, L
cristobalite
CSH (I)
calcite
illite
chlorite
mont. hkl

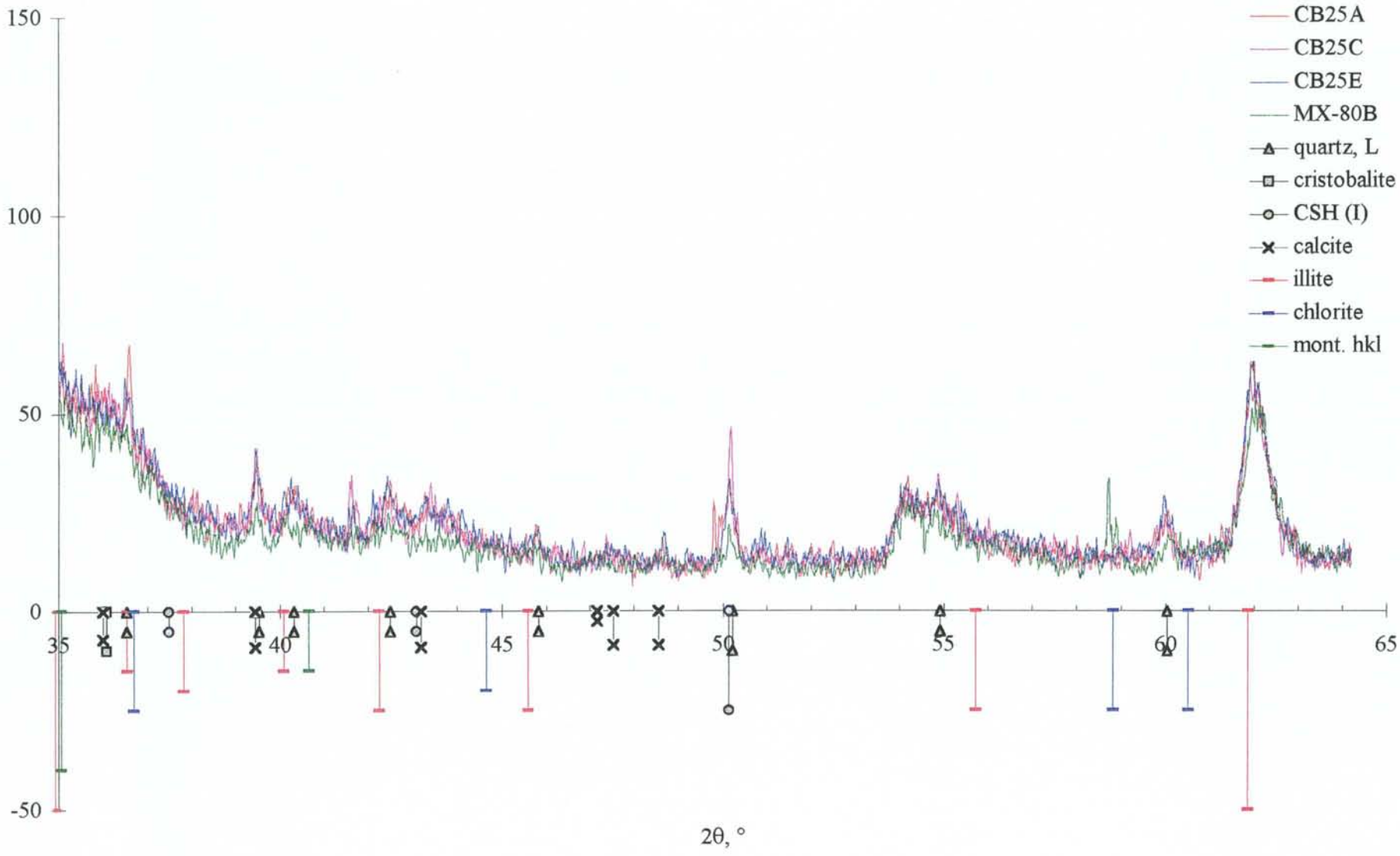
150
100
50
0
-50
35
40
45
50
55
60
65
2θ, °
CB25A
CB25C
CB25E
MX-80B
quartz, L
cristobalite
CSH (I)
calcite
illite
chlorite
mont. hkl

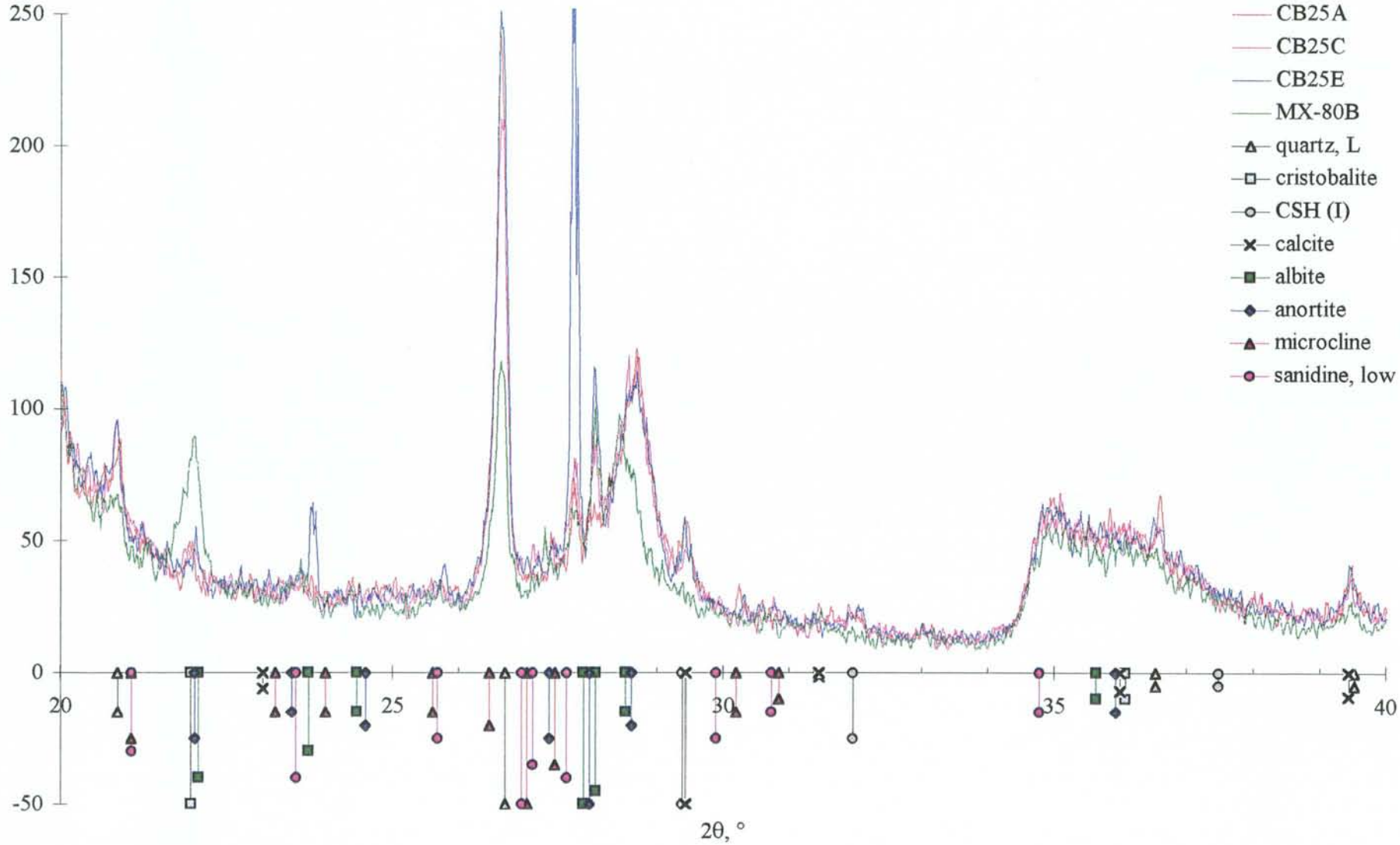
250
200
150
100
50
0
-50
20
25
30
35
40
2θ, °
CB25A
CB25C
CB25E
MX-80B
quartz, L
cristobalite
CSH (I)
calcite
albite
anortite
microcline
sanidine, low

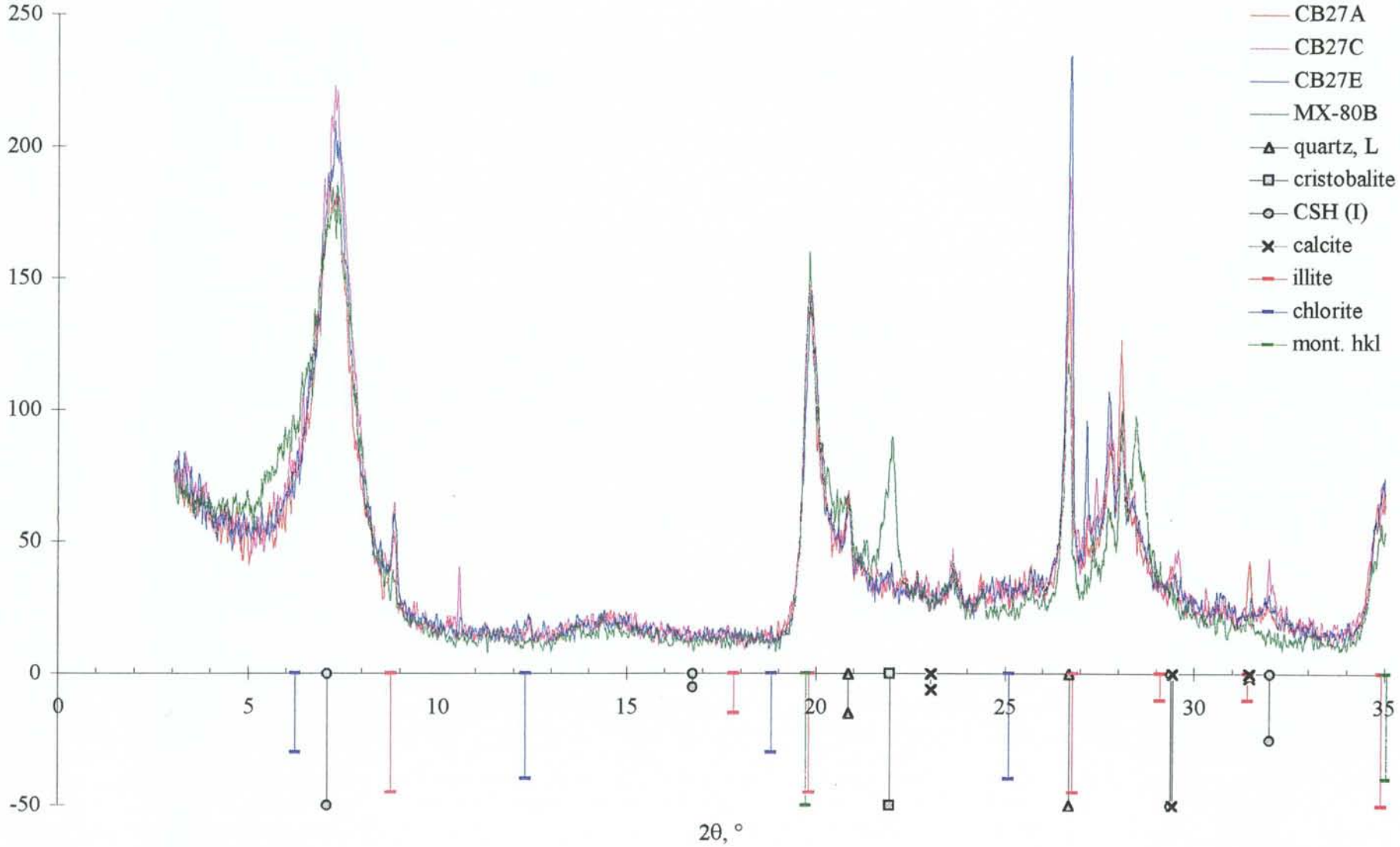
250
200
150
100
50
0
-50
0
5
10
15
20
25
30
35
2θ, °
CB27A
CB27C
CB27E
MX-80B
quartz, L
cristobalite
CSH (I)
calcite
illite
chlorite
mont. hkl

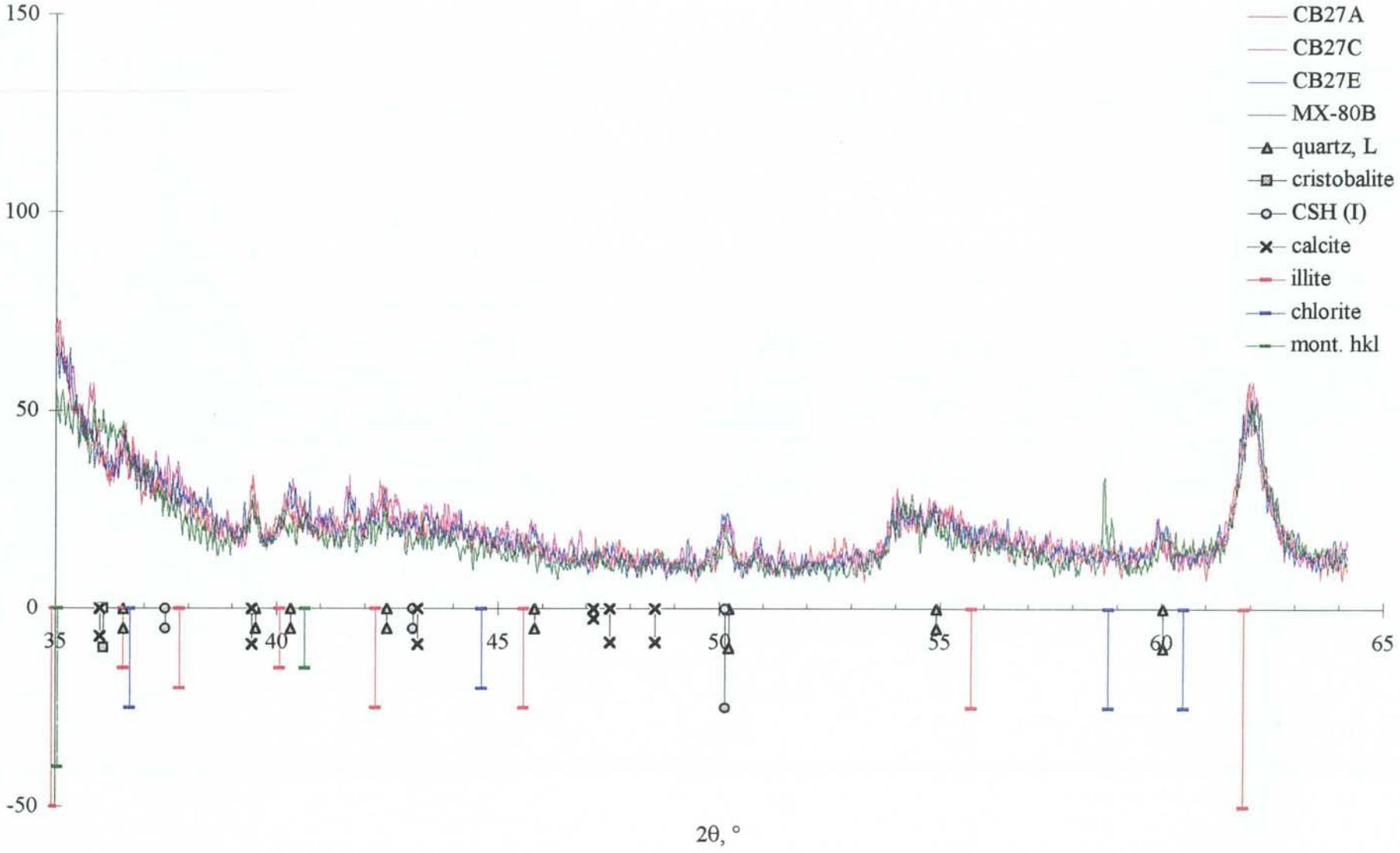
150
100
50
0
-50
35
40
45
50
55
60
65
2θ, °
CB27A
CB27C
CB27E
MX-80B
quartz, L
cristobalite
CSH (I)
calcite
illite
chlorite
mont. hkl

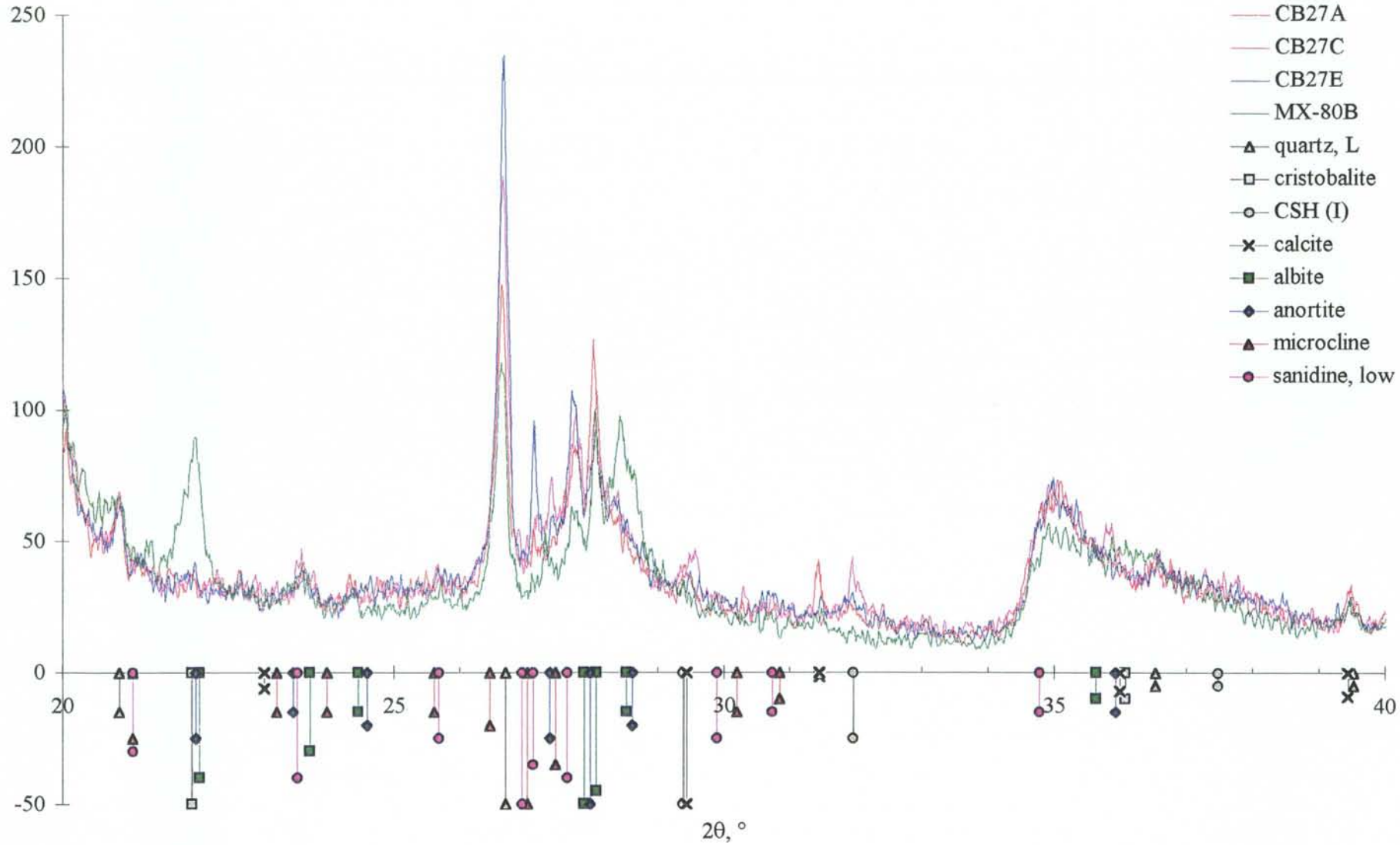
250
200
150
100
50
0
-50
20
25
30
35
40
2θ, °
CB27A
CB27C
CB27E
MX-80B
quartz, L
cristobalite
CSH (I)
calcite
albite
anortite
microcline
sanidine, low

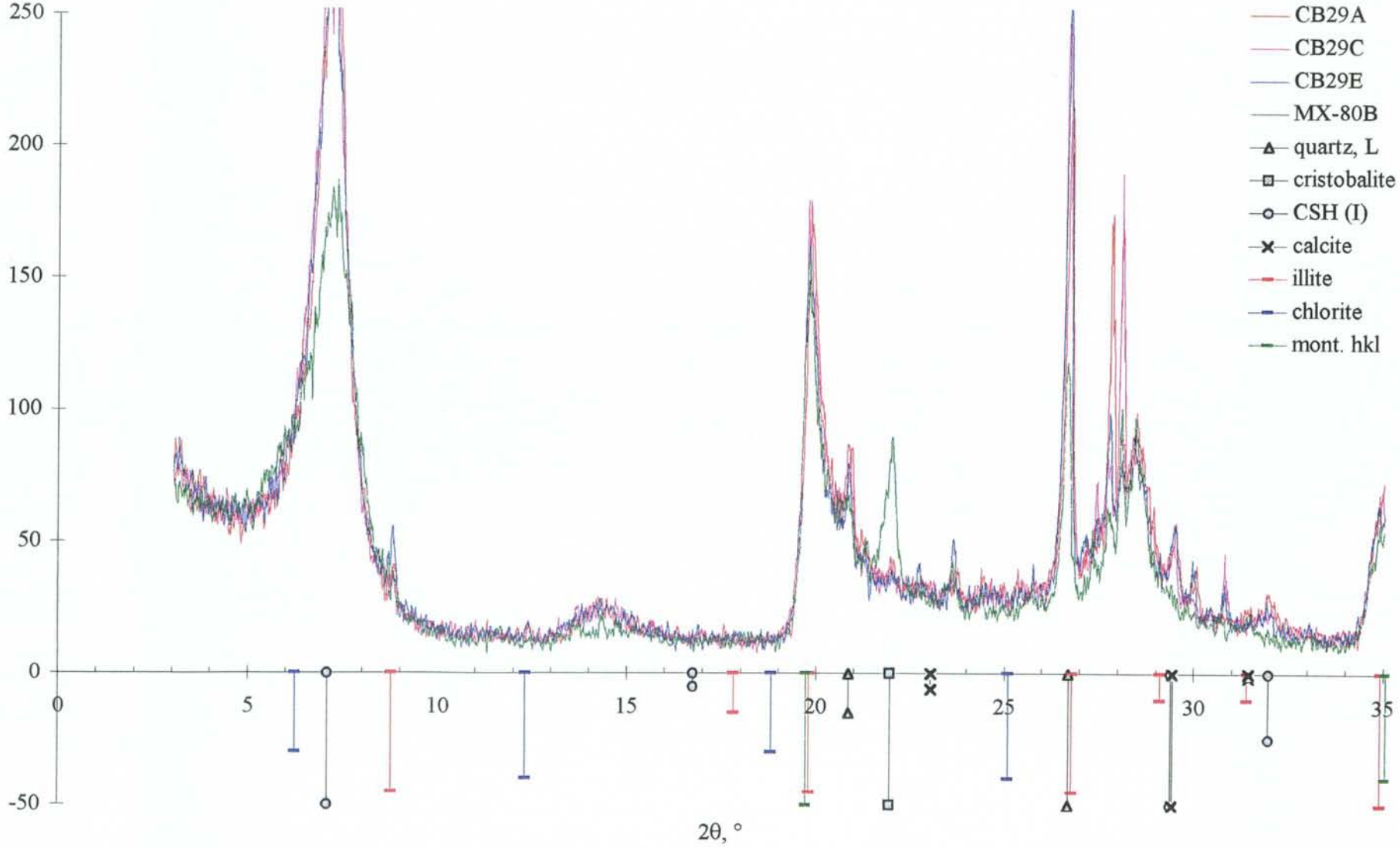
250
200
150
100
50
0
-50
0
5
10
15
20
25
30
35
2θ, °
CB29A
CB29C
CB29E
MX-80B
quartz, L
cristobalite
CSH (I)
calcite
illite
chlorite
mont. hkl

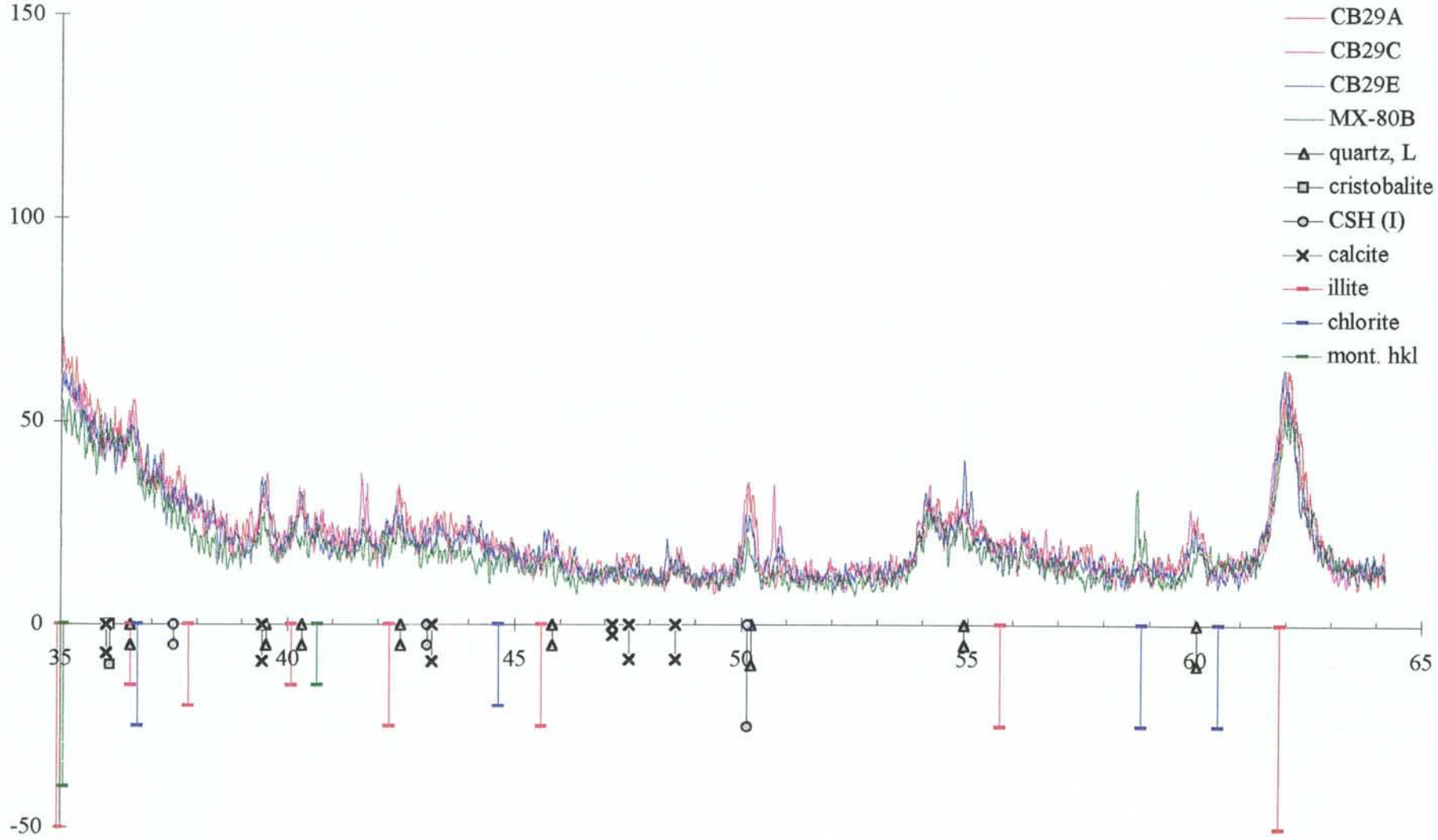
150
100
50
0
-50
35
40
45
50
55
60
65
2θ, °
CB29A
CB29C
CB29E
MX-80B
quartz, L
cristobalite
CSH (I)
calcite
illite
chlorite
mont. hkl

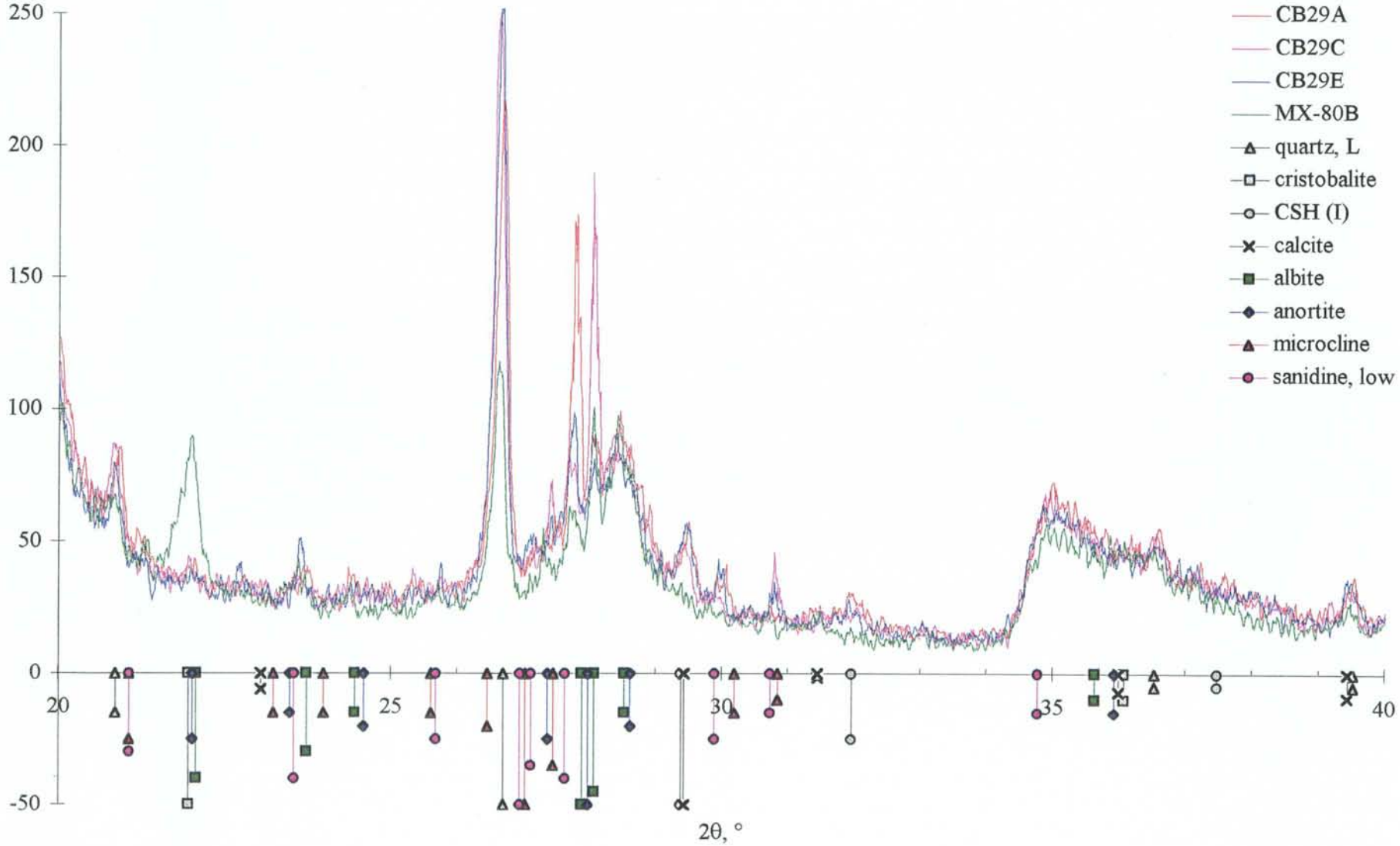
250
200
150
100
50
0
-50
20
25
30
35
40
2θ, °
CB29A
CB29C
CB29E
MX-80B
quartz, L
cristobalite
CSH (I)
calcite
albite
anortite
microcline
sanidine, low

CB 21, 22 analyses test start 93-07-29
sampled 94-11-09
analyzed 94-12-21

mg/liter

	time days	sample	pH	alkalinity mg/l	OH mg/l	Cl mg/l	SO4 mg/l	HCO3 mg/l	Ca mg/l	Fe mg/l	K mg/l	Mg mg/l	Na mg/l			
nask	460	NASK	7.7		0.0085	6390	384	120	800		78	97.2	3220			
nask	460	NASK	7.7		0.0085	6390	384	120	800		78	97.2	3220			
analyzed	time days	sample	pH	alkalinity mg/l	OH mg/l	Cl mg/l	SO4 mg/l	HCO3 mg/l	Ca mg/l	Fe mg/l	K mg/l	Mg mg/l	Na mg/l		S mg/l	Si mg/l
cell sol.	460	CB21	7.58	49	0	6500	390	49	520	0	70	59	3550		123	4.4
cell sol.	460	CB22	10.3	33	3	6200	350	21	548	0	70	34	3500		122	0.2
change		sample	pH	alkalinity mg/l	OH mg/l	Cl mg/l	SO4 mg/l	HCO3 mg/l	Ca mg/l	Fe mg/l	K mg/l	Mg mg/l	Na mg/l		S mg/l	Si mg/l
cell sol.	460	CB21	7.58	49	0	110	6	-71	-280	0	-8	-38	330		123	4
cell sol.	460	CB22	10.3	33	3	-190	-34	-99	-252	0	-8	-63	280		122	0
			molew.	60	17	35.5	96	60	40	56	39	24.3	23		32	28
			charge	-1	-1	-1	-2	-1	2	3	1	2	1		0	0

mmole/l

	time days	sample	pH	alk mmolr/l	OH mmole/l	Cl mmole/l	SO4 mmole/l	HCO3 mmole/l	Ca mmole/l	Fe mmole/l	K mmole/l	Mg mmole/l	Na mmole/l	charge meq/l		
nask	460	NASK	7.7	2	0	180	4	2	20	0	2	4	140	0		
nask	460	NASK	7.7	2	0	180	4	2	20	0	2	4	140	0		
analyzed	time days	sample	pH	alk mmole/l	OH mmole/l	Cl mmole/l	SO4 mmole/l	HCO3 mmole/l	Ca mmole/l	Fe mmole/l	K mmole/l	Mg mmole/l	Na mmole/l	charge meq/l	S mmole/l	Si mmole/l
cell sol.	460	CB21	7.58	0.82	0.00	183.10	4.06	0.82	13.00	0.00	1.79	2.43	154.35	-5.04	3.84	0.16
cell sol.	460	CB22	10.3	0.55	0.20	174.65	3.65	0.35	13.70	0.00	1.79	1.40	152.17	1.68	3.81	0.01
change		sample	pH	alk mmole/l	OH mmole/l	Cl mmole/l	SO4 mmole/l	HCO3 mmole/l	Ca mmole/l	Fe mmole/l	K mmole/l	Mg mmole/l	Na mmole/l	charge meq/l	S mmole/l	Si mmole/l
cell sol.	460	CB21	7.58	-1.18	0.00	3.10	0.06	-1.18	-7.00	0.00	-0.21	-1.57	14.35	-5.04	3.84	0.16
cell sol.	460	CB22	10.3	-1.45	0.20	-5.35	-0.35	-1.65	-6.30	0.00	-0.21	-2.60	12.17	1.68	3.81	0.01

CB 23-29 analyses test start 93-07-29
1 sampled 93-11-01
analyzed 93-12-02

original concentrations, mg/l

position	time	sample	pH	alkalinity	OH	Cl	SO4	HCO3	Ca	Fe	K	Mg	Na	S	Si
valve	days			mg/l	mg/l	mg/l	mg/l	mg/l	mg/l	mg/l	mg/l	mg/l	mg/l	mg/l	mg/l
nask a	ref	-	7.70		0	6390	384	120	800	0	78	97	3220	128	
nask c	ref	-	7.70		0	6390	384	120	800	0	78	97	3220	128	
nask e	ref	-	7.70		0	6390	384	120	800	0	78	97	3220	128	
sulf f	ref	-	13.70		8551	5041	384	0	60	0	17277	0	4761	128	
sulf g	ref	-	13.70		8551	5041	384	0	60	0	17277	0	4761	128	
awp h	ref	-	12.93		1455	5041	384	0	452	0	1248	0	4163	128	
awp i	ref	-	12.93		1455	5041	384	0	452	0	1248	0	4163	128	

raw data concentrations, mg/l

position	time	sample	pH	alkalinity	OH	Cl	SO4	calc. HCO3	Ca	Fe	K	Mg	Na	S	Si
valve	days			mg/l	mg/l	mg/l	mg/l	mg/l	mg/l	mg/l	mg/l	mg/l	mg/l	mg/l	mg/l
nask a	95	27	6.99	110	0	9900	360	110	712	0.1	93	87	5930	129	0.4
nask c	95	29, 25	7.00	130	0	7500	360	130	566	0.3	76	74	4660	182	3
nask e	95	23	6.55	110	0	11000	360	110	697	0.3	75	89	6760	183	1
sulf f	95	27	13.55	26000	6032	5100	390	4711	32	0	13500	0	4530	196	1.4
sulf g	95	29													
awp h	95	25													
awp i	95	23	12.88	4900	1290	4900	390	349	555	0	1030	0	4190	206	0.5

concentration change, mg/l

position	time	sample	pH	alkalinity	OH	Cl	SO4	calc. HCO3	Ca	Fe	K	Mg	Na	S	Si
valve	days			mg/l		mg/l	mg/l	mg/l	mg/l	mg/l	mg/l	mg/l	mg/l	mg/l	mg/l
nask a	95	27	6.99	110	0	3510	-24	-10	-88	0	15	-10	2710	1	0
nask c	95	29, 25	7.00	130	0	1110	-24	10	-234	0	-2	-23	1440	54	3
nask e	95	23	6.55	110	0	4610	-24	-10	-103	0	-3	-8	3540	55	1
sulf f	95	27	13.55	26000	-2519	59	6	4711	-28	0	-3777	0	-231	68	1
sulf g	95	29													
awp h	95	25													
awp i	95	23	12.88	4900	-166	-141	6	349	103	0	-218	0	27	78	1

CB 23-29 analyses test start 93-07-29
2 sampled 94-03-25
analyzed 94-04-29

original position valve	time days	sample	pH	alkalinity mg/l	OH mg/l	Cl mg/l	SO4 mg/l	HCO3 mg/l	Ca mg/l	Fe mg/l	K mg/l	Mg mg/l	Na mg/l	S mg/l	Si mg/l
nask a	ref	-	7.70		0	6390	384	120	800	0	78	97	3220		
nask c	ref	-	7.70		0	6390	384	120	800	0	78	97	3220		
nask e	ref	-	7.70		0	6390	384	120	800	0	78	97	3220		
sulf f	ref	-	13.70		8551	5041	384	0	60	0	17277	0	4761		
sulf g	ref	-	13.70		8551	5041	384	0	60	0	17277	0	4761		
awp h	ref	-	12.93		1455	5041	384	0	452	0	1248	0	4163		
awp i	ref	-	12.93		1455	5041	384	0	452	0	1248	0	4163		

raw data, concentration, calculated

position valve	time days	sample	pH	alkalinity mg/l	OH mg/l	Cl mg/l	SO4 mg/l	HCO3 mg/l	Ca mg/l	Fe mg/l	K mg/l	Mg mg/l	Na mg/l	S mg/l	Si mg/l
nask a	239	27	8.1	75	0	7000	500	75	659	0	152	66	3590	142	44
nask c	239	29, 25	7.0		0										
nask e	239	23	7.0	120	0	6000	400	120	742	0	88	88	3200	142	1
sulf f	239	27	13.4	22000	4270	4000	400	6929	40	0	12100	0	4060	220	6
sulf g	239	29			0										
awp h	239	25	12.8		1073										
awp i	239	23	12.7	5000	852	5000	400	1993	438	0	1020	0	4030	190	1

concentration change calculated

position valve	time days	sample	pH	alkalinity mg/l	OH	Cl mg/l	SO4 mg/l	HCO3 mg/l	Ca mg/l	Fe mg/l	K mg/l	Mg mg/l	Na mg/l	S mg/l	Si mg/l
nask a	239	27	8.10	75	0	610	116	-45	-141	0	74	-31	370	142	44
nask c	239	29, 25	6.95	0	0			-120							
nask e	239	23	7.00	120	0	-390	16		-58	0	10	-9	-20	142	1
sulf f	239	27	13.40	22000	-4281	-1041	16	6929	-20	0	-5177	0	-701	220	6
sulf g	239	29													
awp h	239	25	12.80		-383										
awp i	239	23	12.70	5000	-603	-41	16	1993	-14	0	-228	0	-133	190	1

CB 23-29 analyses test start 93-07-29
3 sampled 94-05-25
analyzed 94-08-03

original

position	time	sample	pH	alkalinity	OH	Cl	SO4	HCO3	Ca	Fe	K	Mg	Na	S	Si
valve	days			mg/l	mg/l	mg/l	mg/l	mg/l	mg/l	mg/l	mg/l	mg/l	mg/l	mg/l	mg/l
nask a	ref	-	7.70		0	6390	384	120	800	0	78	97	3220		
nask c	ref	-	7.70		0	6390	384	120	800	0	78	97	3220		
nask e	ref	-	7.70		0	6390	384	120	800	0	78	97	3220		
sulf f	ref	-	13.70		8551	5041	384	0	60	0	17277	0	4761		
sulf g	ref	-	13.70		8551	5041	384	0	60	0	17277	0	4761		
awp h	ref	-	12.93		1455	5041	384	0	452	0	1248	0	4163		
awp i	ref	-	12.93		1455	5041	384	0	452	0	1248	0	4163		

raw data, concentration, calculated

position	time	sample	pH	alkalinity	OH	Cl	SO4	HCO3	Ca	Fe	K	Mg	Na	S	Si
valve	days			mg/l	mg/l	mg/l	mg/l	mg/l	mg/l	mg/l	mg/l	mg/l	mg/l	mg/l	mg/l
nask a	300	27	7.3	130	0	11000	420	130	734	0	94	89	6170	145	9
nask c	300	29, 25	7.1	98	0	12000	430	98	750	0	76	94	6000	136	0.6
nask e	300	23	7.2	97	0	12000	410	97	737	0	76	93	5990	133	0.7
sulf f	300	27	13.3	25000	3471	4800	410	12750	59	0	14000	0	4600	145	1.5
sulf g	300	29													
awp h	300	25													
awp i	300	23	12.7	4800	852	4700	420	1793	439	0.1	1050	0	3960	130	0.3

concentration change calculated

position	time	sample	pH	alkalinity	OH	Cl	SO4	HCO3	Ca	Fe	K	Mg	Na	S	Si
valve	days			mg/l		mg/l	mg/l	mg/l	mg/l	mg/l	mg/l	mg/l	mg/l	mg/l	mg/l
nask a	300	27	7.25	130	0	4610	36	10	-66	0	16	-8	2950	145	9
nask c	300	29, 25	7.14	98	0	5610	46	-22	-50	0	-2	-3	2780	136	1
nask e	300	23	7.17	97	0	5610	26	-23	-63	0	-2	-4	2770	133	1
sulf f	300	27	13.31	25000	-5080	-241	26	12750	-1	0	-3277	0	-161	145	2
sulf g	300	29													
awp h	300	25													
awp i	300	23	12.70	4800	-603	-341	36	1793	-13	0	-198	0	-203	130	0

CB 23-29 analyses test start 93-07-29
4 sampled 94-08-12
analyzed 94-08-25

original position valve	time days	sample	pH	alkalinity mg/l	OH mg/l	Cl mg/l	SO4 mg/l	HCO3 mg/l	Ca mg/l	Fe mg/l	K mg/l	Mg mg/l	Na mg/l	S mg/l	Si mg/l
nask a	ref	-	7.70		0	6390	384	120	800	0	78	97	3220		
nask c	ref	-	7.70		0	6390	384	120	800	0	78	97	3220		
nask e	ref	-	7.70		0	6390	384	120	800	0	78	97	3220		
sulf f	ref	-	13.70		8551	5041	384	0	60	0	17277	0	4761		
sulf g	ref	-	13.70		8551	5041	384	0	60	0	17277	0	4761		
awp h	ref	-	12.93		1455	5041	384	0	452	0	1248	0	4163		
awp i	ref	-	12.93		1455	5041	384	0	452	0	1248	0	4163		

raw data, concentration, calculated

position valve	time days	sample	pH	alkalinity mg/l	OH mg/l	Cl mg/l	SO4 mg/l	HCO3 mg/l	Ca mg/l	Fe mg/l	K mg/l	Mg mg/l	Na mg/l	S mg/l	Si mg/l
nask a	379	27	11.7	3300	85	6200	450	2999	31	0.03	1180	2	4690	277	596
nask c	379	29, 25													
nask e	379	23	7.0	120	0	6200	360	120	636	0.6	86	76	3270	168	3
sulf f	379	27	13.4	24000	4270	5300	510	8929	26	0.1	13900	0	4590	224	3.5
sulf g	379	29													
awp h	379	25													
awp i	379	23	12.6	4400	677	5000	350	2011	296	0.05	959	0.2	3830	264	1.5

concentration change calculated

position valve	time days	sample	pH	alkalinity mg/l	OH	Cl mg/l	SO4 mg/l	HCO3 mg/l	Ca mg/l	Fe mg/l	K mg/l	Mg mg/l	Na mg/l	S mg/l	Si mg/l
nask a	379	27	11.70	3300	85	-190	66	2879	-769	0	1102	-95	1470	277	596
nask c	379	29, 25		0				-120							
nask e	379	23	6.95	120	0	-190	-24	0	-164	1	8	-21	50	168	3
sulf f	379	27	13.40	24000	-4281	259	126	8929	-34	0	-3377	0	-171	224	4
sulf g	379	29													
awp h	379	25													
awp i	379	23	12.60	4400	-778	-41	-34	2011	-156	0	-289	0	-333	264	2

CB 23-29 analyses test start 93-07-29
5 sampled 94-11-09
analyzed 94-12-21

original

position	time	sample	pH	alkalinity	OH	Cl	SO4	HCO3	Ca	Fe	K	Mg	Na	S	Si
valve	days			mg/l	mg/l	mg/l	mg/l	mg/l	mg/l	mg/l	mg/l	mg/l	mg/l	mg/l	mg/l
nask a	ref	-	7.70		0	6390	384	120	800	0	78	97	3220		
nask c	ref	-	7.70		0	6390	384	120	800	0	78	97	3220		
nask e	ref	-	7.70		0	6390	384	120	800	0	78	97	3220		
sulf f	ref	-	13.70		8551	5041	384	0	60	0	17277	0	4761		
sulf g	ref	-	13.70		8551	5041	384	0	60	0	17277	0	4761		
awp h	ref	-	12.93		1455	5041	384	0	452	0	1248	0	4163		
awp i	ref	-	12.93		1455	5041	384	0	452	0	1248	0	4163		

raw data, concentration,

position	time	sample	pH	alkalinity	OH	Cl	SO4	HCO3	Ca	Fe	K	Mg	Na	S	Si
valve	days			mg/l	mg/l	mg/l	mg/l	mg/l	mg/l	mg/l	mg/l	mg/l	mg/l	mg/l	mg/l
nask a	468	27	9.83	80	1	4300	250	76	343	0.01	256	29	2230	106	25
nask c	468	29, 25	7.05	100	0	5900	350	100	719	0.02	85	84	2930	121	0.34
nask e	468	23	7.10	140	0	5900	370	140	745	0.05	80	86	3040	130	0.4
sulf f	468	27	13.10	25000	2140	4400	330	17446	27	0	13700	0	4280	134	8.8
sulf g	468	29	13.33	26000	3635	4600	350	13172	16	0.02	13900	0.2	4410	175	11
awp h	468	25	12.63	4800	725	4800	370	2241	357	0.02	1010	0.1	4020	140	0.8
awp i	468	23	12.37	5300	399	4900	360	3893	357	0.03	1000	0.2	3940	137	0.7

concentration change

position	time	sample	pH	alkalinity	OH	Cl	SO4	HCO3	Ca	Fe	K	Mg	Na	S	Si
valve	days			mg/l		mg/l	mg/l	mg/l	mg/l	mg/l	mg/l	mg/l	mg/l	mg/l	mg/l
nask a	468	27	9.83	80	1	-2090	-134	-44	-457	0	178	-68	-990	106	25
nask c	468	29, 25	7.05	100	0	-490	-34	-20	-81	0	7	-13	-290	121	0
nask e	468	23	7.10	140	0	-490	-14	20	-55	0	2	-11	-180	130	0
sulf f	468	27	13.10	25000	-6411	-641	-54	17446	-33	0	-3577	0	-481	134	9
sulf g	468	29	13.33		-4916	-441	-34	13172	-44	0	-3377	0	-351	175	11
awp h	468	25	12.63		-730	-241	-14	2241	-95	0	-238	0	-143	140	1
awp i	468	23	12.37	5300	-1057	-141	-24	3893	-95	0	-248	0	-223	137	1

Data from the element analyses of all samples. The element values are related only to the total amount of elements, i.e. corrected for the loss of ignition (LOI). Section A represents the "cement" side of the samples.

SAMPLE	SiO2	Al2O3	CaO	Fe2O3	K2O	MgO	MnO	Na2O	P2O5	TiO2	LOI	SiO2/ Al2O3
MX-80 Na	65.5	20.3	0.84	4.33	0.54	2.59	0.02	4.28	0.09	0.19	6.40	3.23
CB21A	63.6	20.1	6.25	4.28	0.64	2.55	0.02	2.89	0.09	0.19	7.80	3.17
CB21B	66.2	20.2	2.25	4.58	0.69	2.85	0.03	2.69	0.09	0.20	6.10	3.27
CB21C	67.7	20.5	1.59	4.56	0.71	2.65	0.03	2.61	0.10	0.20	5.70	3.31
CB23A	64.1	20.9	2.32	4.78	0.88	3.40	0.03	3.34	0.09	0.20	7.00	3.07
CB23B	65.2	20.4	2.19	5.05	0.98	2.91	0.04	3.25	0.10	0.21	6.40	3.19
CB23C	64.9	20.4	2.42	5.33	1.05	2.78	0.04	3.23	0.11	0.21	6.50	3.18
CB23D	65.5	20.4	1.96	5.11	0.95	2.69	0.04	3.14	0.09	0.20	6.10	3.20
CB23E	66.6	20.7	1.50	5.01	0.93	2.66	0.03	3.10	0.10	0.21	6.10	3.22
CB25A	66.7	21.0	1.50	4.57	0.63	3.16	0.03	3.10	0.08	0.22	6.10	3.18
CB25B	66.8	21.0	1.45	4.73	0.65	2.83	0.03	3.10	0.09	0.20	5.90	3.18
CB25C	66.6	20.7	1.59	4.89	0.72	2.74	0.03	3.07	0.09	0.21	5.90	3.22
CB25D	66.5	20.8	1.58	4.89	0.71	2.75	0.03	3.07	0.10	0.20	5.90	3.19
CB25E	66.5	21.1	1.50	4.88	0.69	2.76	0.03	3.09	0.09	0.20	6.00	3.16
CB27A	61.8	20.9	1.89	4.83	5.64	3.13	0.03	1.66	0.08	0.20	6.90	2.95
CB27B	62.0	21.9	1.40	4.70	5.50	3.13	0.02	1.63	0.08	0.19	6.50	2.83
CB27C	62.8	21.2	1.33	4.86	5.23	3.01	0.03	1.69	0.09	0.20	6.30	2.95
CB27D	63.0	20.9	1.56	5.20	5.10	2.87	0.04	1.77	0.09	0.22	6.40	3.01
CB27E	63.5	21.7	1.12	4.74	5.10	2.91	0.02	1.68	0.08	0.19	6.30	2.93
CB29A	65.5	20.9	1.58	4.78	1.54	3.03	0.03	3.04	0.09	0.20	6.20	3.13
CB29B	66.0	21.4	1.37	4.72	1.46	3.01	0.02	3.04	0.08	0.20	6.00	3.08
CB29C	65.3	20.5	1.77	4.99	1.57	2.79	0.03	2.97	0.09	0.21	6.00	3.18
CB29D	65.3	20.5	1.89	5.18	1.63	2.72	0.04	2.95	0.10	0.21	6.00	3.18
CB29E	65.6	20.7	1.67	5.01	1.62	2.72	0.03	2.96	0.09	0.21	5.90	3.16

Cation exchange capacity (CEC) in the various sections of all analyzed samples. The analyses were made on the clay fraction. Section A represents the "cement" side of the samples.

SPECI-MEN	TEST TYPE	SOLU-TION	CEC meq/100g	Na^+ meq/100g	Ca^{2+} meq/100g	K^+ meq/100g	SEC meq/100g
MX80-c	ref		108.0	62.7	36.0	1.9	100.6
CB21A	Hydro.	NASK	121.4	56.9	62.2	2.1	121.3
CB21B	Hydro.	NASK	117.0	75.9	36.6	2.1	114.6
CB21C	Hydro.	NASK	128.5	63.0	88.9	2.2	154.1
CB23A	Perc.	AWP	134.4	97.5	33.3	7.4	138.2
CB23B	Perc.	AWP	128.3	93.1	31.0	6.8	130.9
CB23C	Perc.	AWP	135.8	90.5	28.4	6.5	125.4
CB23D	Perc.	AWP	134.5	102.4	27.1	7.0	136.5
CB23E	Perc.	AWP	123.0	91.9	18.5	6.1	116.5
CB25A	Diff.	AWP	141.4	88.5	37.9	3.9	130.2
CB24B	Diff.	AWP	121.6	85.3	32.1	3.4	120.8
CB25C	Diff.	AWP	136.8	88.6	21.5	4.1	114.2
CB25D	Diff.	AWP	161.4	84.0	28.9	3.6	116.5
CB25E	Diff.	AWP	154.1	85.0	22.9	3.8	111.7
CB27A	Perc.	SULF	125.2	26.2	21.8	70.9	118.9
CB27B	Perc.	SULF	114.4	28.3	21.9	68.0	118.2
CB27C	Perc.	SULF	118.8	27.6	17.3	72.9	117.8
CB27D	Perc.	SULF	114.4	28.1	17.9	67.2	113.2
CB27E	Perc.	SULF	116.5	31.7	15.4	78.1	125.2
CB29A	Diff.	SULF	123.0	88.3	35.0	20.5	143.8
CB29B	Diff.	SULF	126.9	71.6	26.6	18.4	116.6
CB29C	Diff.	SULF	141.7	86.6	23.2	19.5	129.3
CB29D	Diff.	SULF	145.0	78.4	24.0	18.4	120.9
CB29E	Diff.	SULF	128.2	61.4	17.4	13.4	92.3

List of SKB reports

Annual Reports

1977-78
TR 121
KBS Technical Reports 1 – 120
Summaries
Stockholm, May 1979

1979
TR 79-28
The KBS Annual Report 1979
KBS Technical Reports 79-01 – 79-27
Summaries
Stockholm, March 1980

1980
TR 80-26
The KBS Annual Report 1980
KBS Technical Reports 80-01 – 80-25
Summaries
Stockholm, March 1981

1981
TR 81-17
The KBS Annual Report 1981
KBS Technical Reports 81-01 – 81-16
Summaries
Stockholm, April 1982

1982
TR 82-28
The KBS Annual Report 1982
KBS Technical Reports 82-01 – 82-27
Summaries
Stockholm, July 1983

1983
TR 83-77
The KBS Annual Report 1983
KBS Technical Reports 83-01 – 83-76
Summaries
Stockholm, June 1984

1984
TR 85-01
Annual Research and Development Report 1984
Including Summaries of Technical Reports Issued during 1984. (Technical Reports 84-01 – 84-19)
Stockholm, June 1985

1985
TR 85-20
Annual Research and Development Report 1985
Including Summaries of Technical Reports Issued during 1985. (Technical Reports 85-01 – 85-19)
Stockholm, May 1986

1986
TR 86-31
SKB Annual Report 1986
Including Summaries of Technical Reports Issued during 1986
Stockholm, May 1987

1987
TR 87-33
SKB Annual Report 1987
Including Summaries of Technical Reports Issued during 1987
Stockholm, May 1988

1988
TR 88-32
SKB Annual Report 1988
Including Summaries of Technical Reports Issued during 1988
Stockholm, May 1989

1989
TR 89-40
SKB Annual Report 1989
Including Summaries of Technical Reports Issued during 1989
Stockholm, May 1990

1990
TR 90-46
SKB Annual Report 1990
Including Summaries of Technical Reports Issued during 1990
Stockholm, May 1991

1991
TR 91-64
SKB Annual Report 1991
Including Summaries of Technical Reports Issued during 1991
Stockholm, April 1992

1992
TR 92-46
SKB Annual Report 1992
Including Summaries of Technical Reports Issued during 1992
Stockholm, May 1993

1993
TR 93-34
SKB Annual Report 1993
Including Summaries of Technical Reports Issued during 1993
Stockholm, May 1994

1994

TR 94-33

SKB Annual Report 1994

Including Summaries of Technical Reports Issued during 1994

Stockholm, May 1995

1995

TR 95-37

SKB Annual Report 1995

Including Summaries of Technical Reports Issued during 1995

Stockholm, May 1996

1996

TR 96-25

SKB Annual Report 1996

Including Summaries of Technical Reports Issued during 1996

Stockholm, May 1997

List of SKB Technical Reports 1997

TR 97-01

Retention mechanisms and the flow wetted surface – implications for safety analysis

Mark Elert

Kemakta Konsult AB

February 1997

TR 97-02

Äspö HRL – Geoscientific evaluation 1997/1. Overview of site characterization 1986–1995

Roy Stanfors[1], Mikael Erlström[2], Ingemar Markström[3]

[1] RS Consulting, Lund

[2] SGU, Lund

[3] Sydkraft Konsult, Malmö

March 1997

TR 97-03

Äspö HRL – Geoscientific evaluation 1997/2. Results from pre-investigations and detailed site characterization. Summary report

Ingvar Rhén (ed.)[1], Göran Bäckblom (ed.)[2], Gunnar Gustafson[3], Roy Stanfors[4], Peter Wikberg[2]

[1] VBB Viak, Göteborg

[2] SKB, Stockholm

[3] VBB Viak/CTH, Göteborg

[4] RS Consulting, Lund

May 1997

TR 97-04

Äspö HRL – Geoscientific evaluation 1997/3. Results from pre-investigations and detailed site characterization. Comparison of predictions and observations. Geology and mechanical stability

Roy Stanfors[1], Pär Olsson[2], Håkan Stille[3]

[1] RS Consulting, Lund

[2] Skanska, Stockholm

[3] KTH, Stockholm

May 1997

TR 97-05

Äspö HRL – Geoscientific evaluation 1997/4. Results from pre-investigations and detailed site characterization. Comparison of predictions and observations. Hydrogeology, groundwater chemistry and transport of solutes

Ingvar Rhén[1], Gunnar Gustafson[2], Peter Wikberg[3]

[1] VBB Viak, Göteborg

[2] VBB Viak/CTH, Göteborg

[3] SKB, Stockholm

June 1997

TR 97-06

Äspö HRL – Geoscientific evaluation 1997/5. Models based on site characterization 1986–1995

Ingvar Rhén (ed.)[1], Gunnar Gustafson[2], Roy Stanfors[3], Peter Wikberg[4]

[1] VBB Viak, Göteborg

[2] VBB Viak/CTH, Göteborg

[3] RS Consulting, Lund

[4] SKB, Stockholm

October 1997

TR 97-07

A methodology to estimate earthquake effects on fractures intersecting canister holes

Paul La Pointe, Peter Wallmann, Andrew Thomas, Sven Follin

Golder Associates Inc.

March 1997

TR 97-08

Äspö Hard Rock Laboratory Annual Report 1996

SKB

April 1997

TR 97-09

A regional analysis of groundwater flow and salinity distribution in the Äspö area

Urban Svensson

Computer-aided Fluid Engineering AB

May 1997

TR 97-10
On the flow of groundwater in closed tunnels. Generic hydrogeological modelling of nuclear waste repository, SFL 3–5
Johan G Holmén
Uppsala University/Golder Associates AB
June 1997

TR 97-11
Analysis of radioactive corrosion test specimens by means of ICP-MS. Comparison with earlier methods
R S Forsyth
Forsyth Consulting
July 1997

TR 97-12
Diffusion and sorption properties of radionuclides in compacted bentonite
Ji-Wei Yu, Ivars Neretnieks
Dept. of Chemical Engineering and Technology, Chemical Engineering, Royal Institute of Technology, Stockholm, Sweden
July 1997

TR 97-13
Spent nuclear fuel – how dangerous is it? A report from the project "Description of risk"
Allan Hedin
Swedish Nuclear Fuel and Waste Management Co,
Stockholm, Sweden
March 1997

TR 97-14
Water exchange estimates derived from forcing for the hydraulically coupled basins surrounding Äspö island and adjacent coastal water
Anders Engqvist
A & I Engqvist Konsult HB, Vaxholm, Sweden
August 1997

TR 97-15
Dissolution studies of synthetic soddyite and uranophane
Ignasi Casas[1], Isabel Pérez[1], Elena Torrero[1], Jordi Bruno[2], Esther Cera[2], Lara Duro[2]
[1] Dept. of Chemical Engineering, UPC
[2] QuantiSci SL
September 1997

TR 97-16
Groundwater flow through a natural fracture. Flow experiments and numerical modelling
Erik Larsson
Dept. of Geology, Chalmers University of Technology, Göteborg, Sweden
September 1997

TR 97-17
A site scale analysis of groundwater flow and salinity distribution in the Äspö area
Urban Svensson
Computer-aided Fluid Engineering AB
October 1997

TR 97-18
Release of segregated nuclides from spent fuel
L H Johnson, J C Tait
AECL, Whiteshell Laboratories, Pinawa, Manitoba, Canada
October 1997

TR 97-19
Assessment of a spent fuel disposal canister. Assessment studies for a copper canister with cast steel inner component
Alex E Bond, Andrew R Hoch, Gareth D Jones, Aleks J Tomczyk, Richard M Wiggin, William J Worraker
AEA Technology, Harwell, UK
May 1997

TR 97-20
Diffusion data in granite Recommended values
Yvonne Ohlsson, Ivars Neretnieks
Department of Chemical Engineering and Technology, Chemical Engineering, Royal Institute of Technology, Stockholm, Sweden
October 1997

TR 97-21
Investigation of the large scale regional hydrogeological situation at Ceberg
Anders Boghammar[1], Bertil Grundfelt[1], Lee Hartley[2]
[1] Kemakta Konsult AB, Sweden
[2] AEA Technology, UK
November 1997

TR 97-22
Investigations of subterranean microorganisms and their importance for performance assessment of radioactive waste disposal. Results and conclusions achieved during the period 1995 to 1997
Karsten Pedersen
Göteborg University, Institute of Cell and Molecular Biology, Dept. of General and Marine Microbiology, Göteborg, Sweden
November 1997

TR 97-23
Summary of hydrogeologic conditions at Aberg, Beberg and Ceberg
Douglas Walker[1], Ingvar Rhén[2], Ioana Gurban[1]
[1] INTERA KB
[2] VBB Viak
October 1997

TR 97-24
Characterization of the excavation disturbance caused by boring of the experimental full scale deposition holes in the Research Tunnel at Olkiluoto
Jorma Autio
Saanio & Riekkola Oy, Helsinki, Finland
September 1997

TR 97-25
The SKB Spent Fuel Corrosion Programme.
An evaluation of results from the experimental programme performed in the Studsvik Hot Cell Laboratory
Roy Forsyth
Forsyth Consulting
December 1997

TR 97-26
Thermoelastic stress due to a rectangular heat source in a semi-infinite medium. Application for the KBS-3 repository
Thomas Probert, Johan Claesson
Depts. of Mathematical Physics and Building Physics, Lund University, Sweden
April 1997

TR 97-27
Temperature field due to time-dependent heat sources in a large rectangular grid. Application for the KBS-3 repository
Thomas Probert, Johan Claesson
Depts. of Mathematical Physics and Building Physics, Lund University, Sweden
April 1997

TR 97-28
A mathematical model of past, present and future shore level displacement in Fennoscandia
Tore Påsse
Sveriges geologiska undersökning, Göteborg Sweden
December 1997

TR 97-29
Regional characterization of hydraulic properties of rock using well test data
David Wladis, Patrik Jönsson, Thomas Wallroth
Department of Geology, Chalmers University of Technology, Göteborg, Sweden
November 1997

TR 97-30
ZEDEX - A study of damage and disturbance from tunnel excavation by blasting and tunnel boring
Simon Emsley[1], Olle Olsson[2], Leif Stenberg[2], Hans-Joachim Alheid[3], Stephen Falls[4]
[1] Golder Associates, Maidenhead, United Kingdom
[2] Swedish Nuclear Fuel and Waste Management Co., Figeholm, Sweden
[3] Federal Institute for Geosciences and Natural Resources, Hannover, Germany
[4] Queens University, Kingston, Ontario, Canada
December 1997

TR 97-31
Bentonite swelling pressure in strong NaCl solutions. Correlation between model calculations and experimentally determined data
Ola Karnland
Clay Technology, Lund, Sweden
December 1997